Electronic Supplementary Information (ESI)

for

LMCT transition-based red-light photochemotherapy using a tumour-selective ferrocenyl iron(III) coumarin conjugate

Tukki Sarkar,[a] Arnab Bhattacharyya,*[b] Samya Banerjee,*[c] Akhtar Hussain*[a]

[a] *Department of Chemistry, Handique Girls' College, Guwahati 781001, Assam, India. [E-mail: akhtariisc@gmail.com for general correspondence].*

[b] *Department of Inorganic and Physical Chemistry, Indian Institute of Science, Bangalore 560 012, Karnataka, India. [E-mail: arnab.bhattacharyya1@gmail.com for general correspondence].*

[c] *Institute of Inorganic Chemistry, Georg-August-Universität Göttingen, Tammannstr. 4, 37077 Göttingen, Germany. [E-mail: sbanerj1@uni-goettingen.de for general correspondence].*

Experimental details

Materials

Unless specified, all reagents and chemicals used in this research were procured from commercial sources and used without purification. Solvents were purified before use by standard methods.[S1] Tris-(hydroxymethyl)aminomethane-HCl (Tris-HCl, pH = 7.2) and phosphate buffer saline (PBS, pH = 7.2) buffer solutions was prepared using deionized and sonicated double distilled water. 6,7-dihydroxycoumarin (esculetin), Dulbecco's Modified Eagle's medium (DMEM), Hoechst 33258, 3-(4,5-dimethylthiazol-2-yl)-2,5-diphenyltetrazolium bromide (MTT) and 2',7'-dichlorofluorescein diacetate (DCFDA), propidium iodide (PI), superoxide dismutase (SOD), catalase, tiron and 9,10-anthracenediyl-bis(methylene)dimalonic acid (ABDA) were procured from Sigma-Aldrich (USA) and used as received. Mito-Tracker Red was procured from Invitrogen, USA. Peroxide test strips for the colorimetric detection of peroxide were obtained from Sigma (Merck-Millipore, 110011). Ferrocenyl-*N,N*-bis((pyridin-2-yl)methyl)methanamine ligand (L) was prepared by a literature procedure.[S2]

Measurements

The elemental analyses were carried out on a Thermo Finnigan Flash EA 1112 CHNS analyzer. The infra red (IR) spectra of pure solid samples were recorded on a Bruker ATR FT-IR spectrometer. The UV-Visible absorption spectra were recorded on a Perkin-Elmer Lambda 650 spectrophotometer. The molar conductivity measurements were done using a properly calibrated digital conductivity meter (Labtronics, India). Room temperature electrochemical measurements were carried out using CHI 645D electrochemical workstation, CH instrument, USA with a three-electrode setup consisting of glossy carbon working electrode, platinum wire auxiliary electrode and saturated calomel reference electrode (SCE) at a scan rate of 50 mVs^{-1}. The electrochemical measurements were made using solutions of the metal complexes prepared in HPLC grade DMF solvent. Tetrabutylammonium perchlorate (TBAP, 0.1M) was used as a supporting electrolyte in DMF. The electrospray ionization mass spectra (ESI-MS) were recorded using Agilent Technologies 6538 UHD Accurate-mass Q-TOF LC/MS mass spectrometer. The fluorescence quantum yield was determined using a PerkinElmer LS 55 fluorescence spectrometer with coumarin-153 laser dye as a reference with a known quantum yield (Φ) value of 0.56 in acetonitrile.[S3] The samples for quantum yield determination were prepared in

acetonitrile and deaerated prior to measurements. The sample and the reference were excited at 395 nm, maintaining nearly equal absorbances. The integrated emission intensity was calculated using Origin Pro 8.1 software and the quantum yield was calculated using the equation $\Phi_S/\Phi_R = (A_S/A_R) \times [(OD)_R/(OD)_S] \times [(n_S)^2/(n_R)^2]$, where, Φ_S and Φ_R are the fluorescence quantum yields of the sample and reference respectively, A_S and A_R are the area under the fluorescence spectra of the sample and the reference respectively, $(OD)_S$ and $(OD)_R$ are the respective optical densities of the sample and the reference solution at the wavelength of excitation, and n_S and n_R are the respective refractive indices of the solvents used for the sample and the reference.[S4,S5] Room temperature magnetic susceptibilities of the DMSO-d_6 solutions of the Fe(III) complexes containing 1% TMS (v/v) as the internal reference were obtained by a solution NMR method with a Bruker AMX-400 NMR spectrometer.[S6,S7] The magnetic moments were calculated by the Evans method using the equation: $\mu_{eff} = 0.0618(\Delta fT/fM)$, where Δf is the observed shift in frequency of the TMS signal, T is the temperature (K), f is the operating frequency (MHz) of the NMR spectrometer, and M is the molarity of the complex in the solution.[S8] The confocal microscopic investigations were carried out using Olympus FV 3000 confocal microscope. The flow cytometric analysis was performed using FACS Calibur (Becton Dickinson (BD) cell analyzer) at FL1 channel (595 nm).

Syntheses of complexes 1 and 2

The complexes were synthesized by a general procedure. Anhydrous $FeCl_3$ (0.16 g, 1 mmol) was dissolved in 1:2 (v/v) methanol/acetone mixture (5 mL) to which a solution of the dipicolylamine ligand L (0.4 g, 1.0 mmol) taken in the same solvent mixture (5 ml) was added drop wise. The solution was brought to its reflux temperature and the respective catecholate ligand (catechol, 0.11 g; esculetin, 0.18 g, 1.0 mmol), previously dissolved methanol (5 mL) and neutralized by triethylamine (0.202 g, 2.0 mmol), was added slowly to the reaction mixture. The resulting mixture was further refluxed for 30 min and then filtered to remove any insoluble materials and the filtrate was cooled to room temperature. Diethyl ether (25 mL) was slowly added to the filtrate whereupon a dark violet solid of the complex precipitated. The precipitate was filtered, washed with ice-cold methanol (10 ml) and finally dried in vacuum over P_4O_{10}.

[Fe(L)(cat)Cl] (**1**): Yield: ~77%. Anal. calcd for $C_{29}H_{27}N_3O_2ClFe_2$: C, 58.37; H, 4.56; N, 7.04. Found: C, 58.51; H, 4.52; N, 7.00. ESI–MS in methanol: *m/z* 561.0782 $[M–Cl^-]^+$. FT–IR data (solid sample)/ cm^{-1}: 2986 w, 2690 w, 1602 m, 1464 s, 1445 m, 1307 w, 1248 vs,

1160 m, 1101 m, 1023 s, 944 w, 807 m, 768 m, 738 s, 630 m (w, weak; m, medium, s, strong; vs, very strong). UV–visible in 1:9 v/v DMF-PBS [λ_{max}/nm (ε/ M^{-1} cm^{-1})]: 270 (12,500), 345 sh (2,700), 468 (1,800), 758 (1,830). Molar conductivity in DMF at 298 K [Λ_M / S cm^2 mol^{-1}]: 82. μ_{eff} = 5.86μ_B at 298 K.

[Fe(L)(esc)Cl] (**2**): Yield: ~84%. Anal. calcd for $C_{32}H_{27}N_3O_4ClFe_2$: C, 57.82; H, 4.09; N, 6.32. Found: C, 57.93; H, 4.15; N, 6.29. ESI–MS in methanol: *m/z* 629.2412 $[M–Cl^-]^+$. FT–IR data (solid sample)/ cm^{-1}: 2989 w, 1660 s, 1602 m, 1572 m, 1464 vs, 1425 m, 1368 s, 1268 vs, 1248 s, 1180 m, 1091 w, 1013 m, 915 w, 797 s, 758 m, 699 w, 640 w. UV–visible in 1:9 v/v DMF-PBS [λ_{max}/nm (ε/ M^{-1} cm^{-1})]: 270 (16,600), 391 (12,100), 494 sh (3,690), 720 (2,000). Molar conductivity in DMF at 298 K [Λ_M / S cm^2 mol^{-1}]: 69. μ_{eff} = 5.86μ_B at 298 K.

Lipophilicity

Lipophilicity of complexes **1a**, **2a**, catechol and esculetin were measured by determining their partition coefficients (log*P*) between *n*-octanol and water using the conventional shake-flask method.[S9] First, an absorbance calibration plot was constructed for the complex at varying concentrations of the complex in the aqueous medium. Then, known concentration of the aqueous solution of the complex was mixed with equal volume of *n*-octanol. After vortex-shaking the mixture, the two phases were allowed to separate. The remaining concentration of the complex in aqueous phase was then determined from the calibration plot.The partition coefficient was calculated by using the equation log*P* = log$[complex]_{oct}$/$[complex]_{aq}$, where $[complex]_{oct}$ is the concentration of the complex in *n*-octanol phase and $[complex]_{aq}$ is the concentration in the aqueous phase.

X-ray crystallographic procedures

The crystal structure of complex **1** was obtained by the single-crystal X-ray diffraction technique. Single crystals of **1** were grown by slow evaporation of a solution of the complex in methanol. Crystal mounting was done on glass fiber with epoxy cement. All geometric and intensity data were collected at room temperature using an automated Bruker SMART APEX CCD diffractometer equipped with a fine focus 1.75 kW sealed tube Mo-K_α X-ray source (λ = 0.71073 Å) with increasing ω (width of 0.3° per frame) at a scan speed of 4 seconds per frame. Intensity data, collected using ω-2θ scan mode, were corrected for Lorentz–polarization effects and for absorption.[S10] Patterson and Fourier techniques were used to solve the structures and refinement was done by full-matrix least-squares method using

SHELX system of programs.[S11] The hydrogen atoms belonging to the complexes were in their calculated positions and refined using a riding model. All non-hydrogen atoms were refined anisotropically. The perspective views of the molecules were obtained by ORTEP.[S12]

Computational methodology

To rationalize the photophysical properties and to obtain a better understanding of the molecular structure and electronic nature of the complexes, DFT computational studies were performed using B3LYP hybrid functional and LANL2DZ basis-set for all atoms as incorporated in *Gaussian* 09 software package.[S13,S14] In order to ascertain stationary points, frequency tests were performed after optimization of the ground-state structures. The initial coordinates required for the DFT studies were adopted from the crystallographic parameters of the complex **1** and to find the effect of solvent molecules on the respective geometry and frontier orbitals of the complexes, IEF-PCM model was incorporated taking water as the bulk solvent. The optimized coordinates are listed in Table S3-S4.

Cell culture

HeLa (human cervical carcinoma), MCF-7 (human breast adenocarcinoma), HaCaT (human skin keratinocyte), and MCF-10A (human breast epithelial cell) cells were maintained in DMEM supplemented with 10% FBS, 100 IU mL^{-1} of penicillin, 100 µg mL^{-1} of streptomycin and 2 mM of Glutamax at 37 °C in a humidified incubator at 5% CO_2. The adherent cultures were grown as monolayer and were passaged once in 4-5 days (at around 80% confluence) by trypsinizing with 0.25% Trypsin-EDTA.

Confocal microscopy experiments

The cellular permeability and intracellular localization properties of complex **2a** was studied using confocal microscopy. HeLa cells (~ 5×10^4) were cultured overnight in Thermo scientific Nunc 35 mm glass bottom dishes using 10% FBS-DMEM medium. The cells were then incubated with complex **2a** (20 µM of complex **2**) for 4 h and the culture medium was replaced with fresh medium. Mitotracker Red (MTR, 200 µL of 100 nM stock in PBS buffer of pH = 7.2) was then added to the dishes and incubated for 15 minutes. Nucleus targeting blue emissive Hoechst 33258 dye (1 µL from 1 µg/ml stock in PBS buffer, pH = 7.2) was also added to the HeLa cells and incubated for ~10 minutes. The trackers were then washed with PBS and the culture medium was also replaced by PBS buffer. Finally, confocal microscopic experiments were performed using Olympus FV 3000 confocal microscope at

60× magnification. To record the green emission of complex **2a**, the samples were excited using 405 nm blue laser light source. The acquired images were then processed using Olympus cellSens imaging software.

Cytotoxicity

The cytotoxicity of the complexes was studied using MTT assay in light and dark conditions in HeLa, MCF-7, HaCaT and MCF-10A cells following reported procedures.[S15] The MTT assay method is based on the ability of mitochondrial dehydrogenases of viable cells to cleave the tetrazolium rings of MTT, forming dark purple membrane impermeable crystals of formazan that can be estimated from the spectral measurements in DMSO at 540 nm. Photo-irradiation was done with a broad band visible light (400−700 nm, 10 J cm^{-2}) using Luzchem Photoreactor (Model LZC-1, Ontario, Canada, Sylvania fluorescent white tubes with a fluence rate of 2.4 mW cm^{-2} to provide a total dose of 10 J cm^{-2}) or with red light (600-720 nm, power, 50 J cm^{-2}) from a Waldman PDT 1200L photoreactor. The absorbance was measured at 540 nm using a Molecular Devices Spectra Max M5 plate reader. Cytotoxicity of the complexes was measured as the percentage ratio of the absorbance of the treated cells to the untreated controls. The cytotoxicity was expressed in terms of the IC_{50} values which were determined by nonlinear regression analysis using Graph Pad Prism 7.

The ABDA probe for singlet oxygen detection

9,10-anthracenediylbis(methylene)dimalonic acid (ABDA) was used as a probe to detect the generation of singlet oxygen ($^1O_2$) by complex **2a** under visible light irradiation. For this, complex **2** stock solution prepared in DMSO (1 mM) was added to ABDA (1 mM) stock solution in water to obtain a final concentration of 20 μM of ABDA and 10 μM of complex **2**. The decrease in absorbance of the anthracene-centered band of ABDA at 378 nm was at an interval of 10 min of continuous irradiation with visible light (400-700 nm, 10 J cm^{-2}).[S16]

DCFDA assay for ROS generation

DCFDA assay was carried out to detect any generation of intracellular ROS.[S17] Cell permeable 2′,7′-dichlorofluorescein diacetate (DCFDA) on oxidation by cellular ROS generates green fluorescent 2′,7′-dichlorofluorescein (DCF) with an emission maxima around 525 nm.[S18] To detect intracellular ROS generation, HeLa cells were incubated with **2a** (10 μM of complex **2**) for 4 h followed by photo-exposure to visible light (400-700 nm) for 1 h in PBS (50 mM phosphate buffer, pH, 7.2 containing 150 mM NaCl). After harvesting the cells

by trypsinization, a single cell suspension of 1×10^6 cells ml^{-1} was prepared. The cells were then treated with 10 μM DCFDA in dark for 15 min at room temperature. The distribution of the HeLa cells, stained by DCFDA, was determined by FACS analysis. Several other samples were recorded at the same time keeping the cells only control and cells+dye control the same. The control data are previously published with different compounds.[S19,S20] In another experiment using red light, 10 μL of DCFDA stock solution (1.0 mM) was added to 2 mL of complex **2** (20 μM) and 100 μL of PBS was added, and red light (CW diode laser, elliptical beam, wavelength 705 nm, 38 mW, Model LQC705-38E, Newport Corporation, USA) was employed as the irradiation source. The emission of DCFDA at 525 nm was recorded.[24a,S21,S22]

The peroxide colorimetric test for H_2O_2

The peroxide colorimetric tests for the detection of hydrogen peroxide in the reaction medium were conducted by using the Quantofix peroxide test sticks as per the instructions provided by the manufacturer (Merck-Supelco). In a typical experiment, complex **2a** (10 μM of complex **2**) in 1% DMSO/99% PBS (v/v) at room temperature was kept either in the dark or irradiated with visible light (400−700 nm, 10 J cm^{-2}) or red light (CW diode laser, elliptical beam, wavelength 705 nm, 38 mW, Model LQC705-38E, Newport Corporation, USA). Formation of H_2O_2 was detected by immersing an otherwise colorless stick into the reaction medium and then noting any color change after 30 s. Development of a color indicates a positive test for H_2O_2, whereas no color change indicates a negative test for H_2O_2.[3a,S23]

Propidium iodide assay

To visualise the cellular and nuclear morphological changes, PI staining was performed. Approximately 4×10^4 HeLa cells, plated over cover slips in each 6 well plate, were incubated with complex **2a** (15 μM of complex **2**) for 4 h followed by photo-irradiation by visible light (400-700 nm) for 1 h in PBS (50 mM phosphate buffer, pH, 7.2 containing 150 mM NaCl) and 20 h recovery in DMEM-FBS in the dark respectively. Cells were fixed and permeabilized with chilled methanol for 10 min at 20 °C. After removal of methanol and PBS washing, cells were incubated with propidium iodide (10 mg ml^{-1}) to stain the nucleus for 20 min. After three PBS washes, the cells were mounted in 90% glycerol solution containing Mowiol and sealed with a nail painter. Images were acquired using an ApoTome.2 fluorescence microscope (Carl Zeiss, Germany) at 63× magnification.

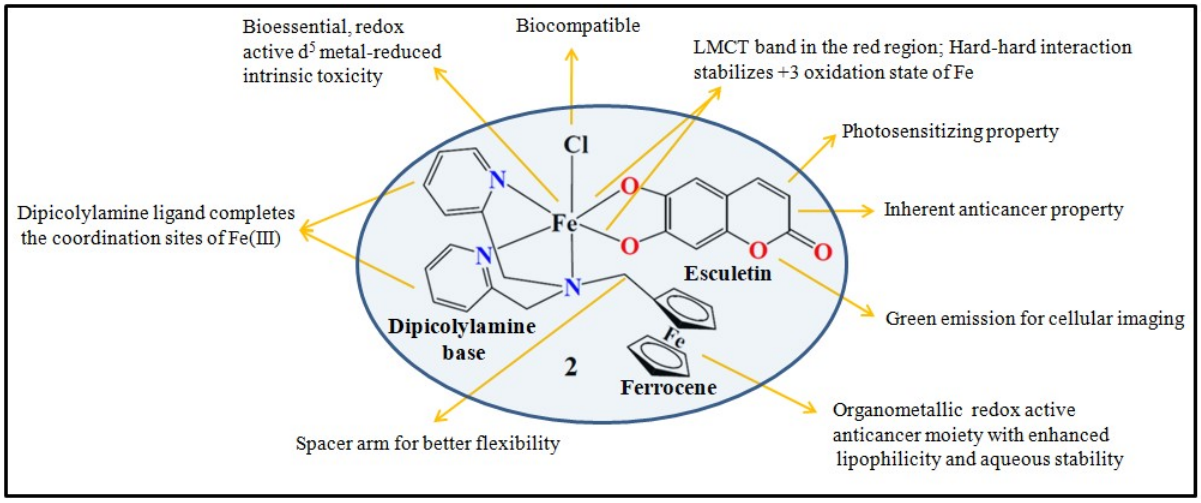

Scheme S1. A schematic representation showing the design aspects of complex **2**.

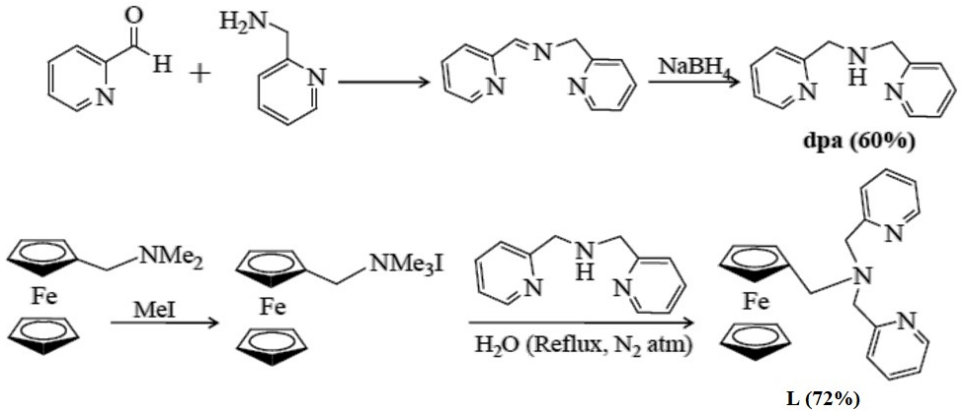

Scheme S2. Synthetic scheme for the preparation of ligand L used in this study.[S2]

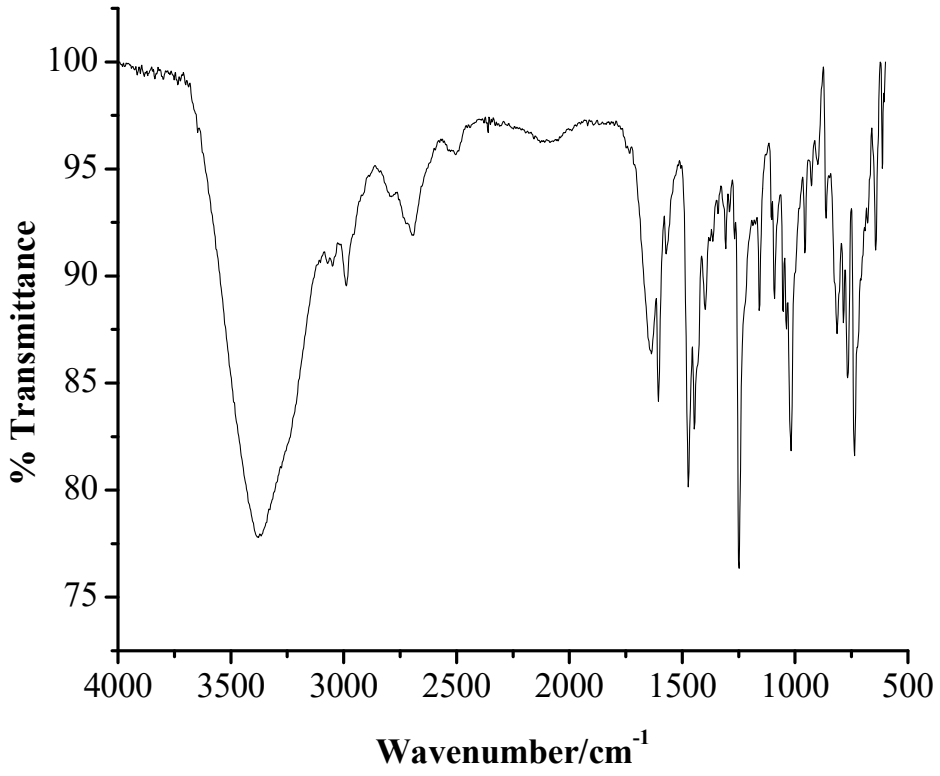

Fig. S1. The solid-state FT-IR spectrum of complex **1**.

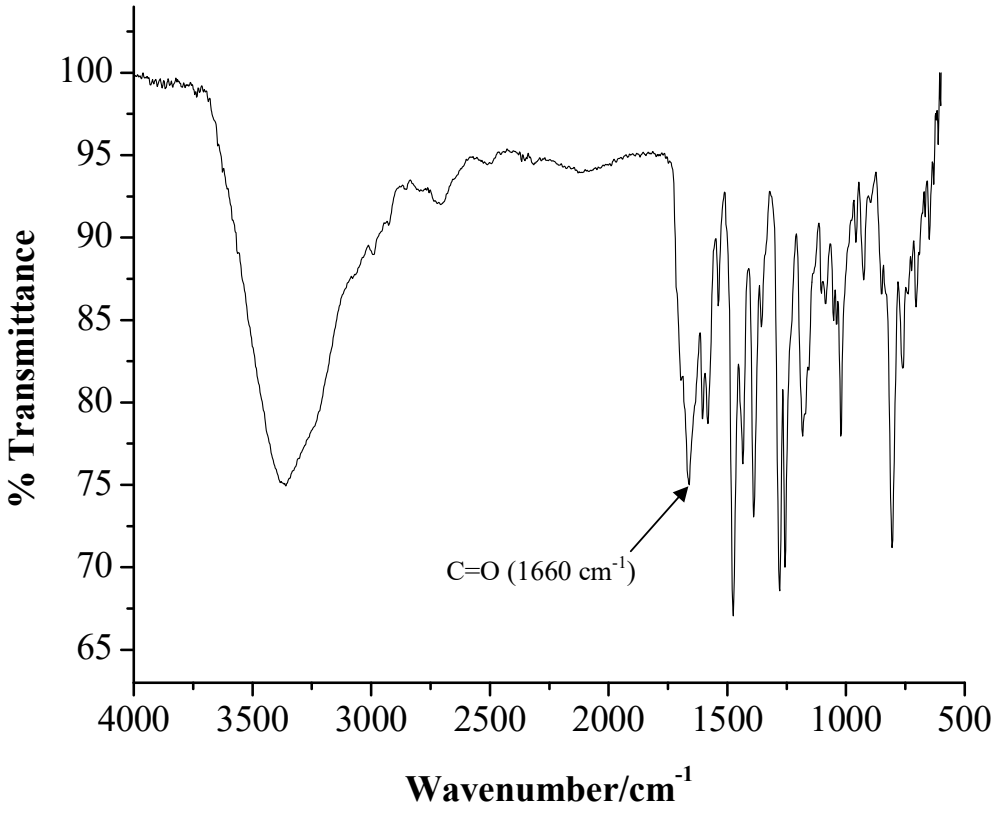

Fig. S2. The solid-state FT-IR spectrum of complex **2**.

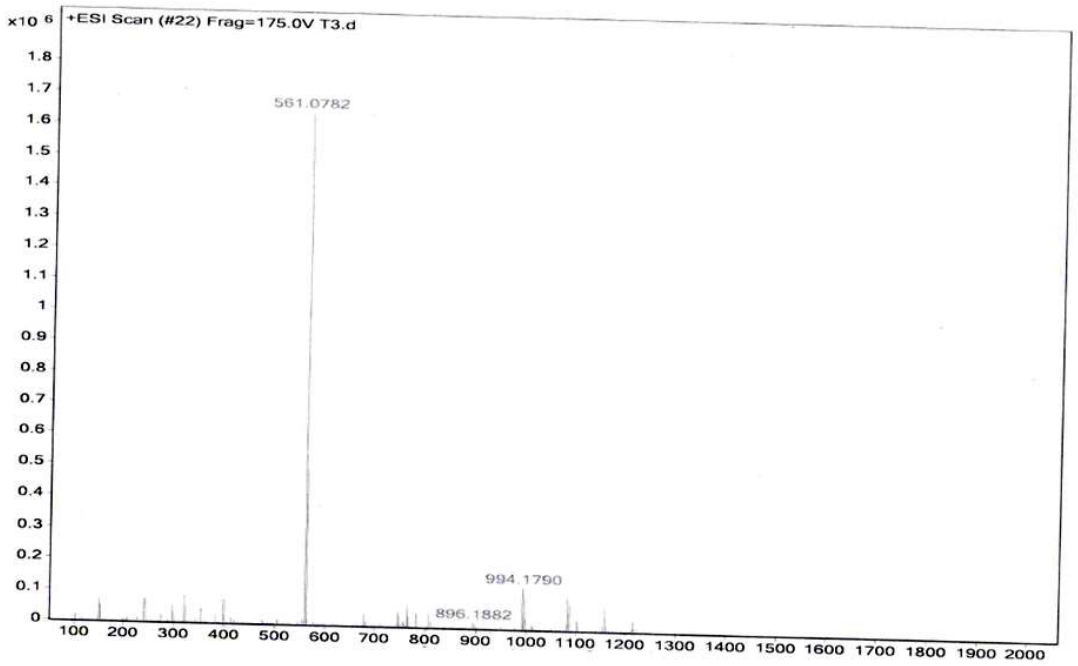

Fig. S3. The ESI-MS (+) spectrum of complex [Fe(L)(cat)(Cl)] (**1**) showing the prominent $[M–(Cl^-)]^+$ peak at m/z = 561.0782.

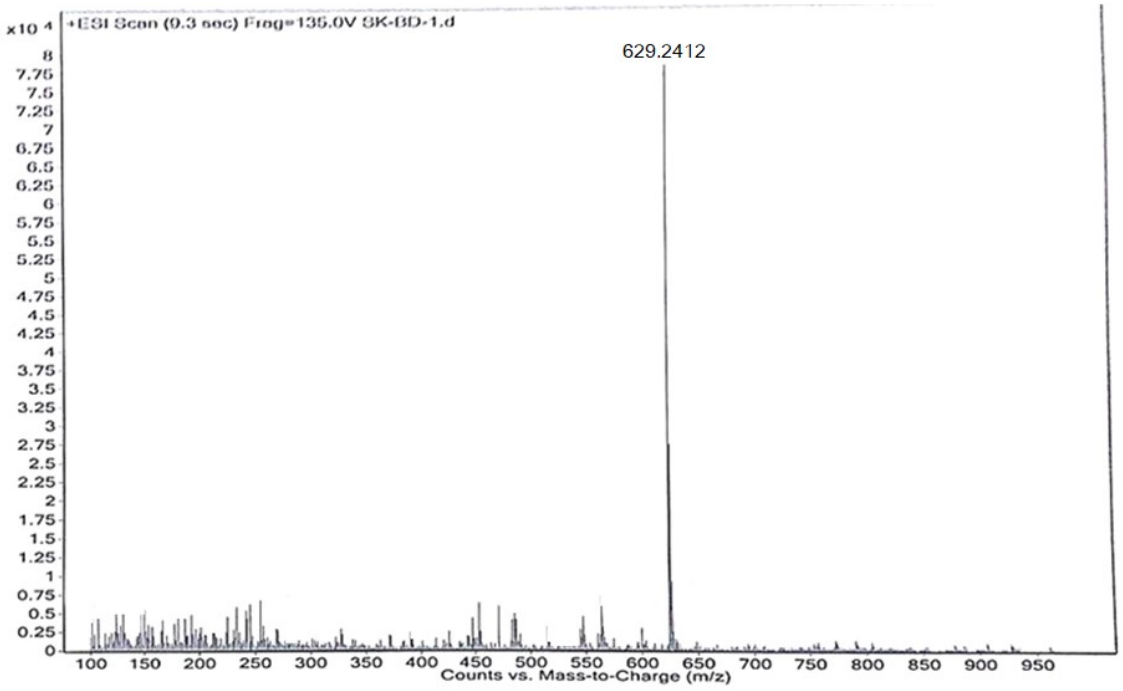

Fig. S4. The ESI-MS (+) spectrum of [Fe(L)(esc)(Cl)] (**2**) showing the prominent $[M–(Cl^-)]^+$ peak at m/z = 629.2412.

Identity of complexes 1 and 2 in aqueous phase

Although complexes **1** and **2** are neutral in the solid state, they behave as 1:1 electrolytes in a solution phase, which is supported by the ESI-MS (Fig. S4 and Fig. S5) and molar conductivity data. In a solution phase, the labile chloride ligand is displaced by a solvent molecule to form $[Fe(L)(cat)(sol]^+$ or $[Fe(L)(esc)(sol)]^+$ (where sol is the solvent used to dissolve the complex). Thus, what we have is essentially a monocationic complex as the actual solution species. The absorption spectra of the complexes were recorded is 1:9 DMF-PBS, therefore it is reasonable to assume that the species in solution is predominantly an aqua complex, namely, $[Fe(L)(cat)(H_2O]^+$ (hence labelled as **1a**) or $[Fe(L)(esc)(H_2O]^+$ (hence labelled as **2a**). Thus, the aqueous chemistry of complexes **1** and **2** are essentially due to the aqua complexes **1a** and **2a** respectively. Similarly, the cytotoxicity and all cell-based assays were conducted in culture media containing only 1% DMSO. Thus the actual species in such experiments is also the monocationic aqua complex. We could not detect the coordinated water ligand in our ESI-MS study, probably due to its rapid exchange with the solvent water molecules. Similarly, crystallization from a methanol solution of complex **1** did not lead to an aqua complex, but rather a chloro complex as described in the manuscript. Furthermore, our several attempts to isolate and obtain the single crystals of the aqua complex were unsuccessful, even after chloride ligand metathesis by $AgClO_4$. However, for a series of structurally analogous iron(III) complexes, Palaniandavar *et al.* have unequivocally demonstrated that the actual species in aqueous solution is the monocationic aqua complex, rather than a neutral complex (references 7c and 7d in the manuscript).[S24]

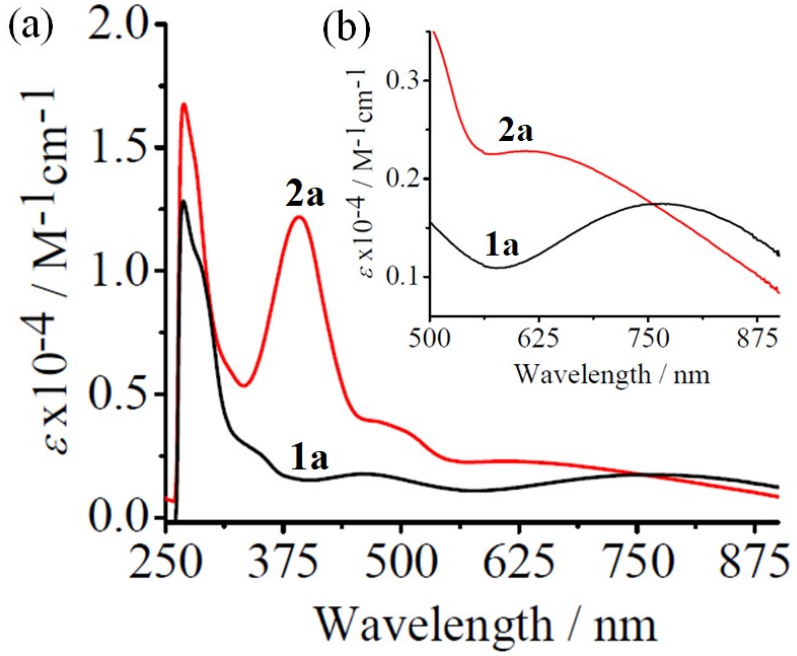

Fig. S5. (a) The electronic absorption spectra of complexes **1a** (black) and **2a** (red) recorded in DMF-PBS (1:9 v/v, pH = 7.2). (b) A magnified representation of the LMCT (catecholate to Fe(III)) absorption bands of complexes **1a** and **2a**.

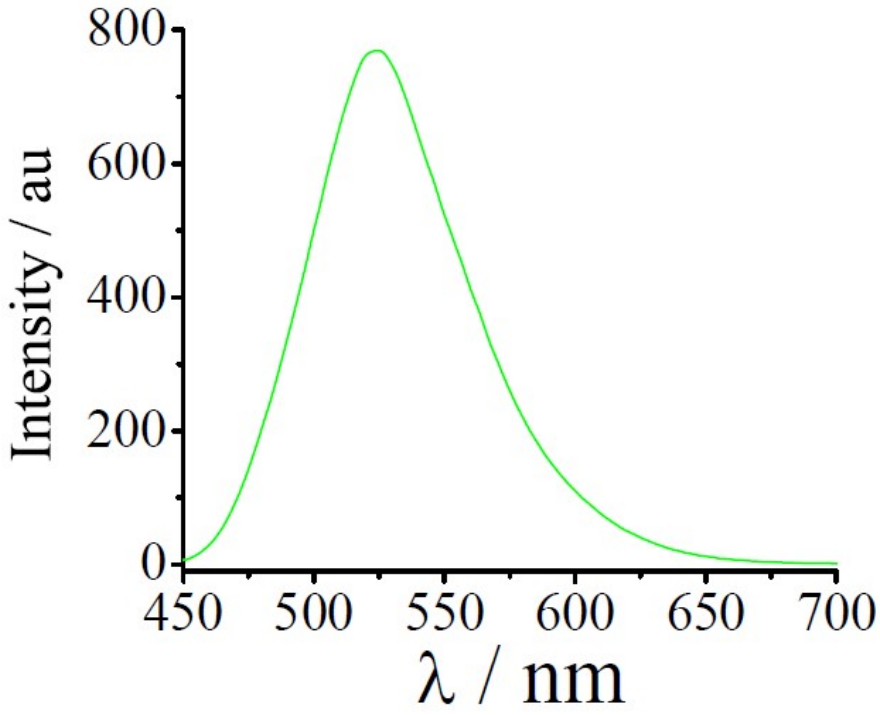

Fig. S6. Fluorescence spectrum of complex **2** in DMF (λ_{ex} = 395 nm, λ_{em} = 525 nm, Φ = 0.02 in acetonitrile).

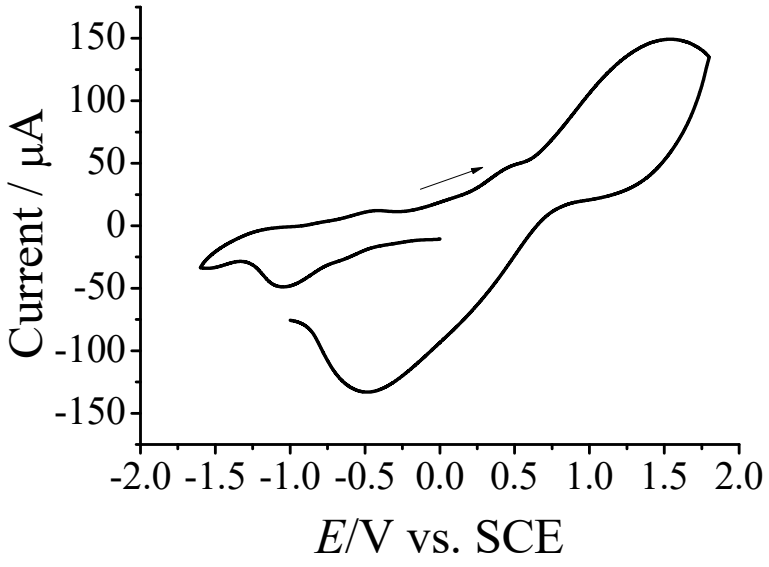

Fig. S7. Cyclic voltammogram of complex **1** recorded in DMF in the presence of 0.1 M TBAP as supporting electrolyte.

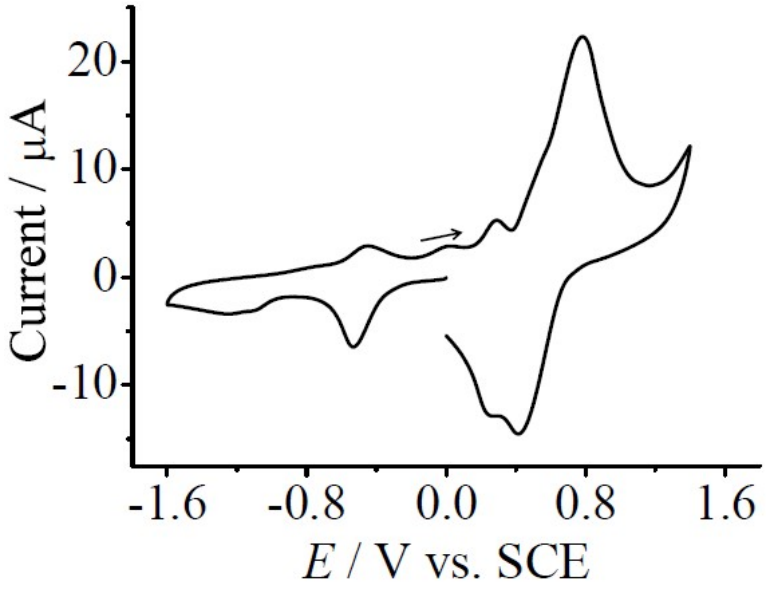

Fig. S8. Cyclic voltammogram of complex **2** recorded in DMF in the presence of 0.1 M TBAP as supporting electrolyte.

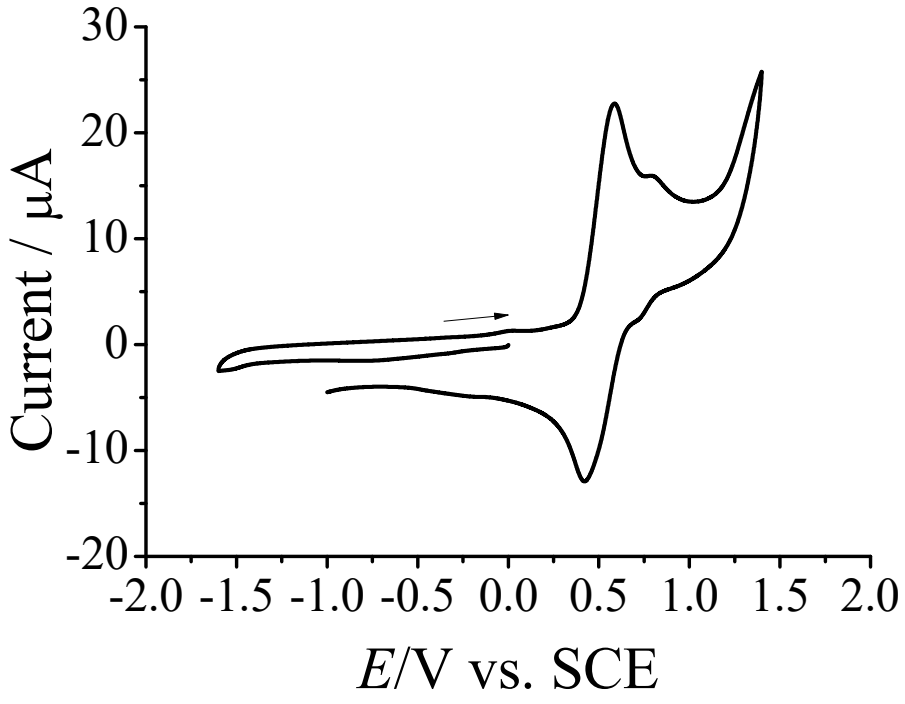

Fig. S9. Cyclic voltammogram of the free ligand L recorded in DMF in the presence of 0.1 M TBAP as supporting electrolyte.

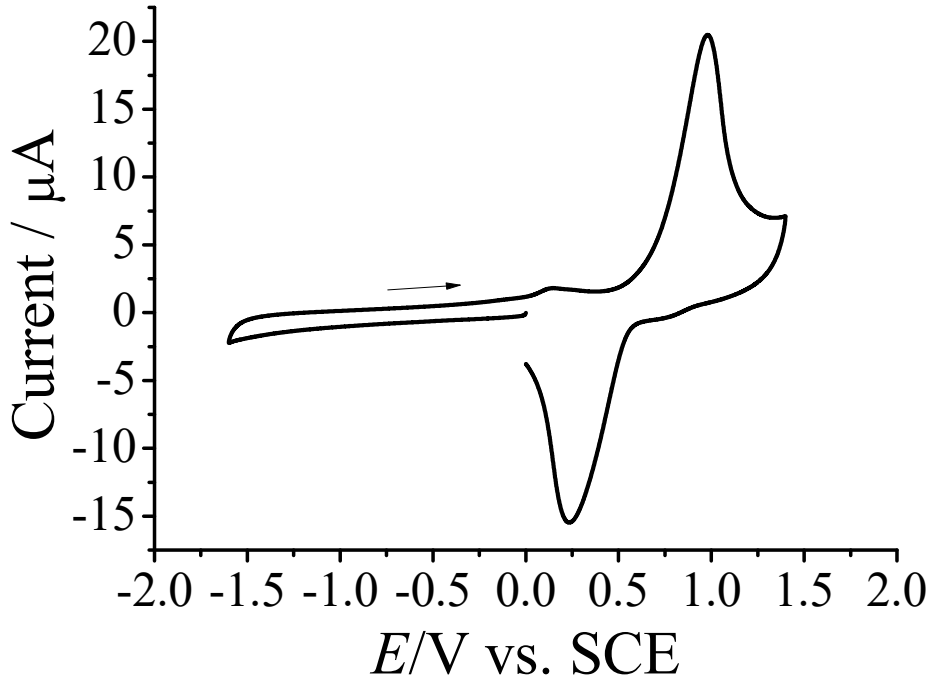

Fig. S10. Cyclic voltammograms of the free esculetin ligand recorded in DMF in the presence of 0.1 M TBAP as supporting electrolyte.

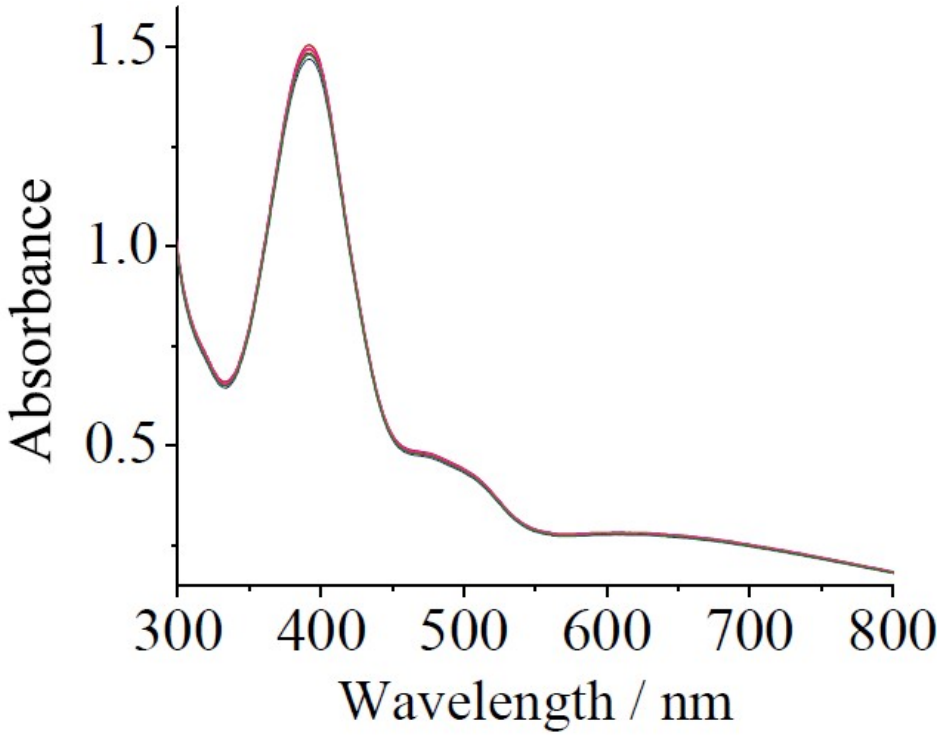

Fig. S11. Time-dependent UV-visible absorption spectral traces of complex **2a** in 10% DMSO–DMEM medium (pH = 7.4, 37 °C) monitored upto 48 h.

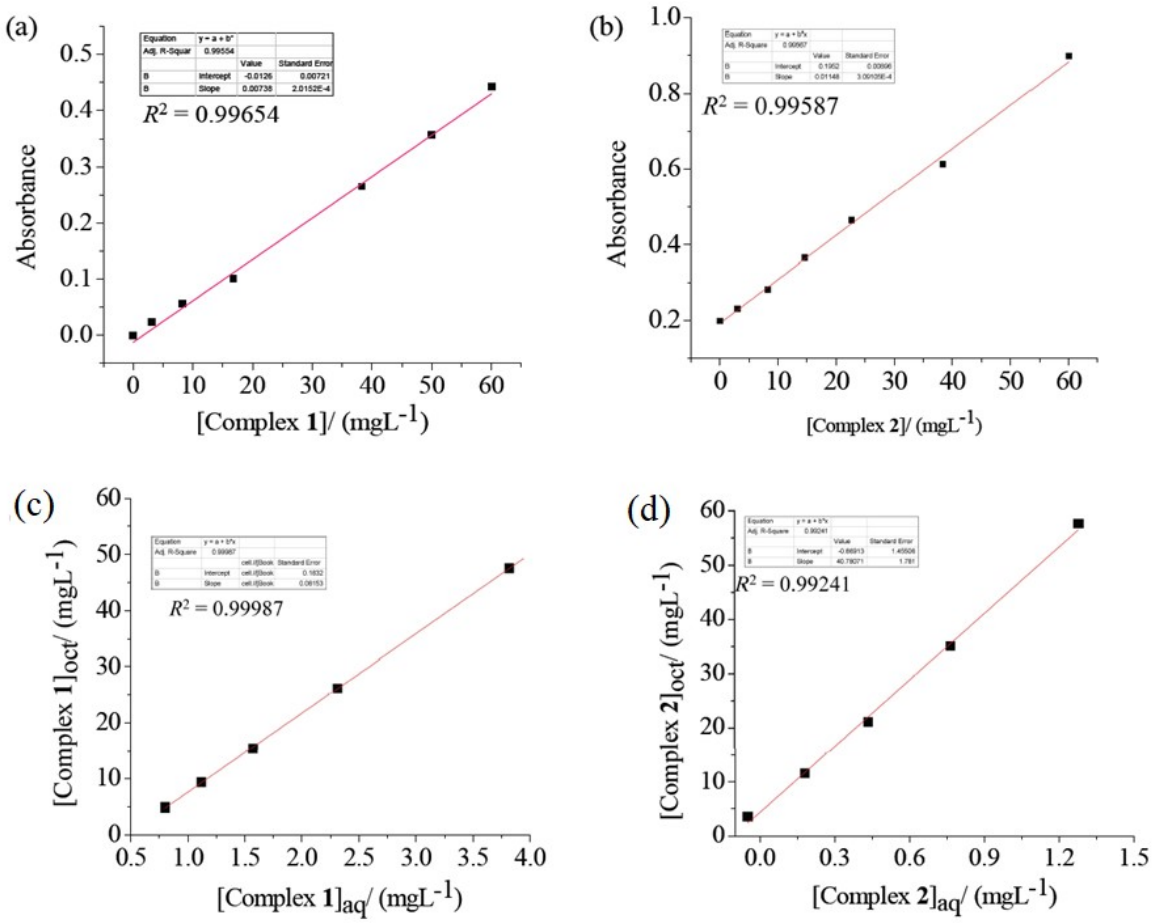

Fig. S12. Calibration plots for (a) complex **1a** and (b) complex **2a** in H_2O; while, plots (b) and (d) are partition coefficient determining plots for complexes **1a** and **2a** respectively.

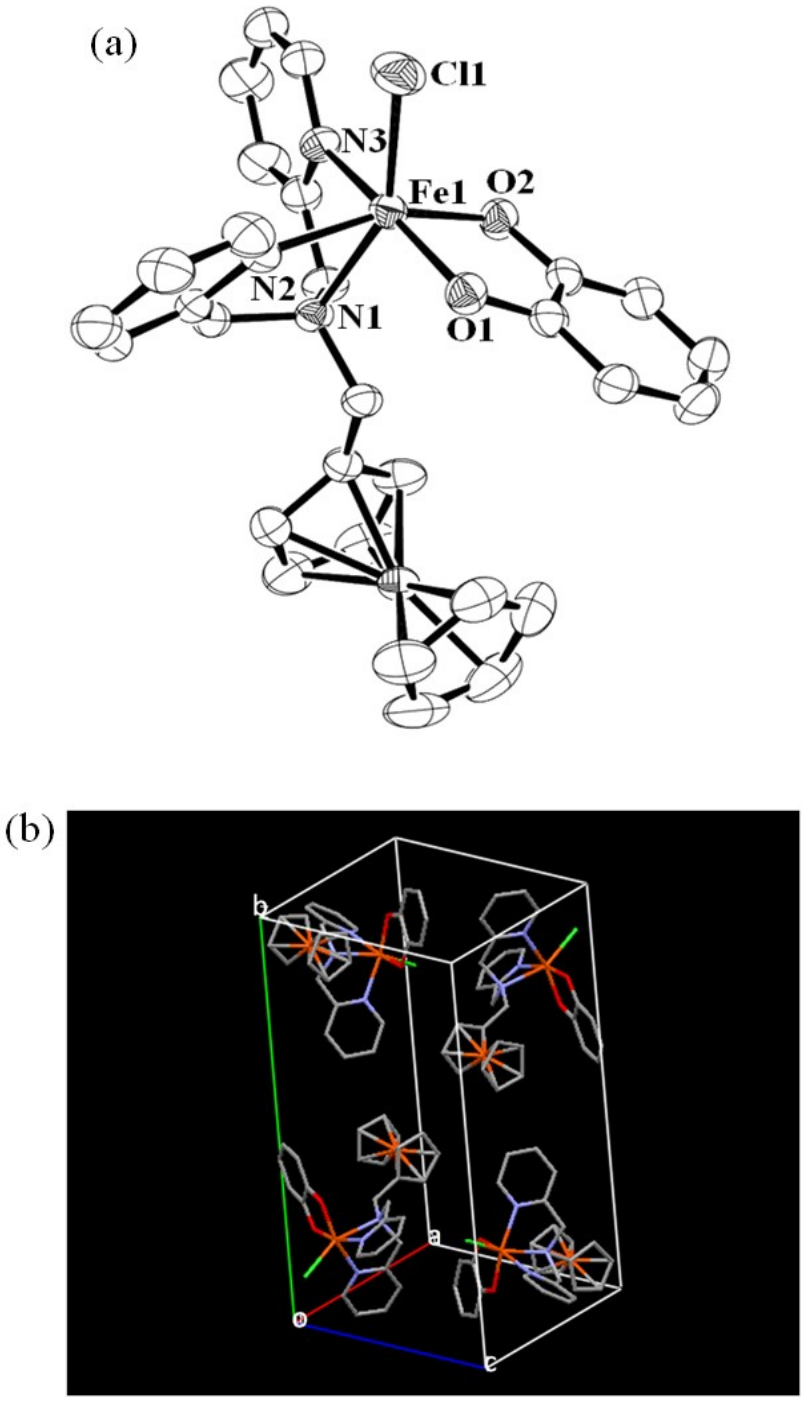

Fig. S13. (a) ORTEP diagram of complex **1** showing 50% thermal ellipsoid probability (H atoms are not shown). (b) The unit cell packing diagram for complex **1** in the solid state.

Discussion on the possibility of existence of isomers of complexes 1 and 2

The following four isomers are theoretically possible for complex **1**. The same is true for complex **2** as well.

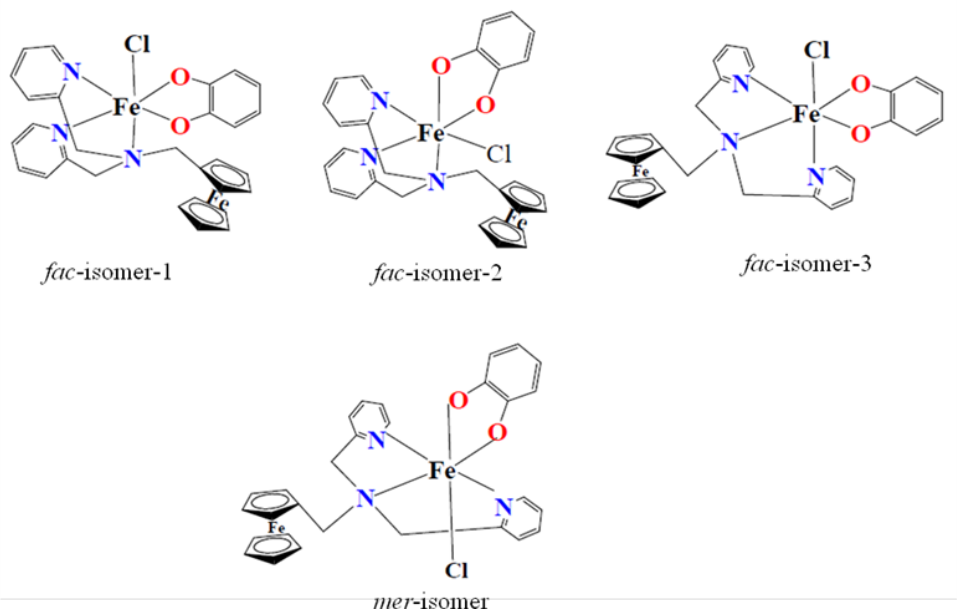

Fig. S14. Four isomeric structures that are theoretically possible for complex **1** (same is applicable for complex **2**).

During the synthesis, complexes **1** and **2** were isolated as brown crystalline materials. Crystallization of this brown solid (complex **1**) from its methanol solution yielded brown block-shaped crystals suitable for single-crystal X-ray diffraction. A careful visual inspection of these single crystals under high-resolution stereozoom and polarizing microscopes revealed exclusively one type of single crystal (the brown block-shaped) of complex **1** in the sample. We did not find any other types of crystals, perhaps with different shapes and color in the sample. This observation led us to the conclusion that only one type of isomer was present in the solid state thereby ruling out the possibility for the presence of other isomeric complexes. The crystal structure of complex **1** shows a distorted octahedral geometry around the iron(III) centre formed by the facially occupied tridentate *N,N,N* donor ligand (L), bidentate *O,O* donor catecholate ligand (cat), and the monodentate chloride (Cl^-). The chloride ligand is *trans* to the central aliphatic *N* atom (sp^3 hybridized) of the tridentate ligand (L), in preference to the pyridyl *N* atoms (sp^2 hybridized). Our observation is also supported by the previously published data by Palaniandavar *et al.* on structurally similar mixed-ligand iron(III) complexes with a tridentate *N,N,N*-donor ligand, and a bidentate *O,O*-donor catecholate ligand (references 7c and 7d in the revised manuscript).[S25] Thus, it is reasonable

to conclude that the tridentate ligand (L) occupies the facial site in preference to a meridional position in the complex. In the present case, the *fac*-isomer-1 is what we have observed in preference to the other three structures. While the *mer*-isomer would be energetically unfavorable, the other two *fac*-isomers could lie significantly higher in energy compared to isomer-1, disfavoring their existence. Thus, in the solid state, the *fac*-isomer-1 (Cl ligand *trans* to the aliphatic N atom of the tridentate ligand L) could be the energetically most favorable one in preference to others. However, in a solution state, the energy difference between the three facial isomers could be marginal thereby allowing their interconversion. Thus, in a solution phase, their simultaneous existence cannot be ruled out.

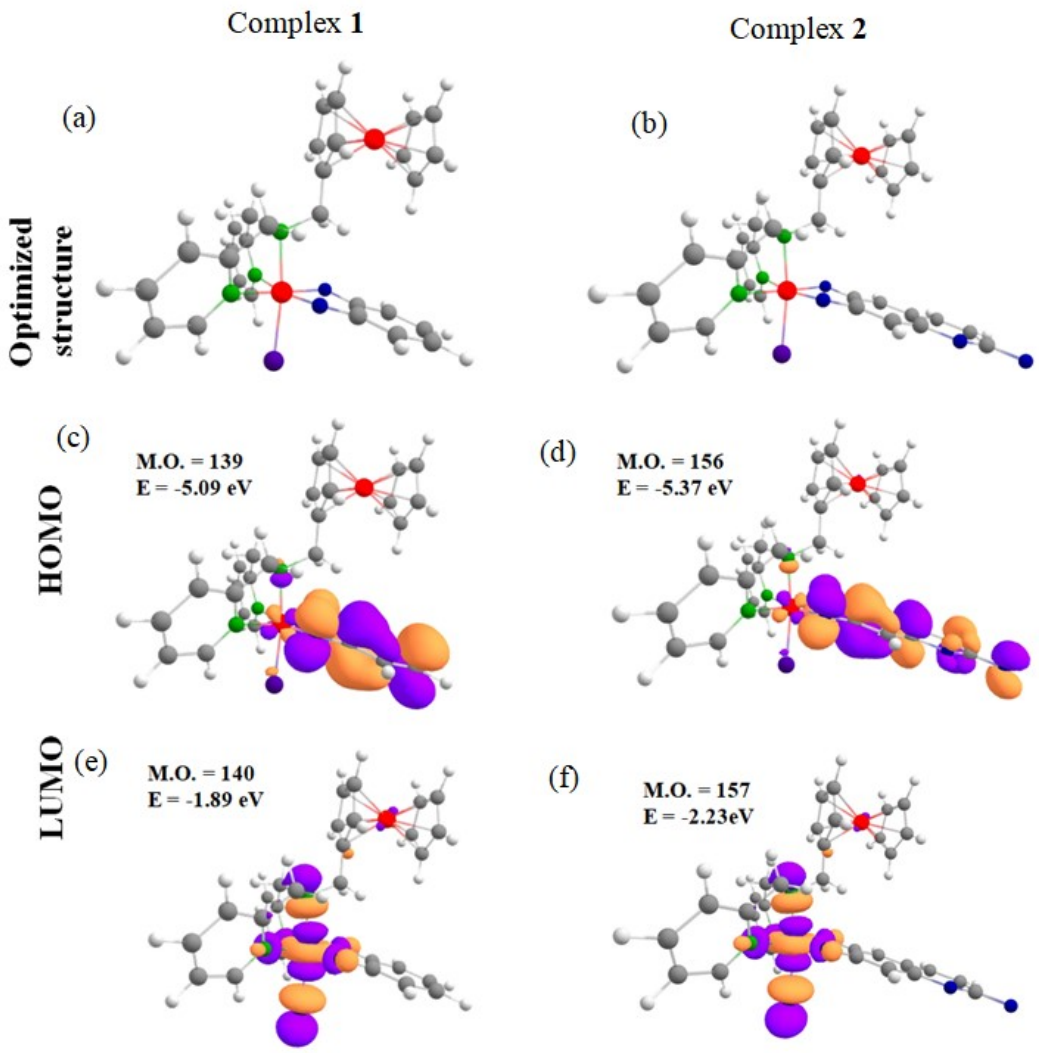

Fig. S15. The DFT optimized structures of complexes **1** and **2** in panels (a) and (b), the HOMOs in panels (c) and (d), and the LUMOs in panels (e) and (f) respectively.

Discussion on the use of red-light for phototoxicity studies

The rationale behind using red light for phototoxicity study is that complexes **1a** and **2a** possess a moderate intensity LMCT band within 600-850 nm (red/NIR region) originating from the catecholate moiety coordinated to iron(III) centre. However, the mere presence of this LMCT band is not enough for a complex to show phototoxicity even when irradiated with red light (in our case we have used PDT source from Waldman 1200 L photoreactor, 600-720 nm). The presence of a photosensitizer ligand is required for a complex to show phototoxicity. Complex **1a** (used as control in our study) has a simple catecholate ligand coordinated to iron(III). But catechol doesn't have any significant photosensitizing property under light irradiation. In contrast, complex **2a** possesses an esculetin ligand instead of the catechol ligand. Esculetin is a naturally occurring coumarin derivative and its structure contains a catecholate unit. But unlike the simple catechol molecule, esculetin is known to act as a photosensitizer (references 9 and 10 in the manuscript). Thus, complex **2a**, in turn, can act as a photosensitizer to elicit a PDT effect when irradiated by red light. Complex **1a** cannot behave as a photosensitizer due to the absence of such photosensitizer ligand, even though it possesses a similar LMCT band in the red region. This type of behavior is well documented in the literature. For example, many oxovanadium(IV), and iron(III) complexes having a photosensitizer ligand are reported to show phototoxicity against cancer cells. But, the corresponding complex with a non-photosensitizer ligand is inactive. For example, dipyridophenazine (dppz) ligand is a known photosensitizer, whereas its simpler analog phenanthroline (phen) is not. Therefore the dppz complexes with oxovanadium(IV) show phototoxicity, but the corresponding phen complexes are inactive though both posses a low energy *d-d* band in the red light region. Similarly, iron(III) complexes with anthracenyl and pyrenyl photosensitizers show red-light phototoxicity but the corresponding phenyl (non-photosensitizer) complex is inactive.[S26-S29]

The position of λ_{max} for the LMCT band in iron(III)-catecholate type complexes is sensitive to the nature of the catecholate ligand. For complex **1a** with a simple catecholate ligand, this band covers the region 600-900 nm. For complex **2a**, this band is in the region 550-850 nm. Esculetin ligand with its extended π conjugated structure is electron-withdrawing in nature. Thus, the charge transfer from the esculetin ligand to iron(III) centre requires slightly more energy (λ_{max} = 720 nm) for complex **2a** in comparison to complex **1a** (λ_{max} = 785 nm) with a simple catecholate ligand (Fig. 1(a) in the manuscript). In addition, for complex **2a**, the LMCT band on the left side (Fig. 1) is significantly masked by the presence of a high-intensity band at 370-440 nm due to the esculetin ligand. But for complex **1a**, the band is

clear on both sides (Fig. S3 above). The effect of the LMCT energy on the nature of the catecholate ligand is well documented in the literature (references 7c and 7d in the manuscript).[S24,S25,S30]

Our idea of using red light is based on the fact that red-light has a longer wavelength than visible light and hence deeper tissue penetration into the tumour and hence better PDT outcome (mentioned in page 1 in the manuscript). Overall, our idea was to design a complex that is photochemotherapeutically active within the PDT spectral window (600-800 nm). The fact that complex **2a** is more active in the visible light is because of the presence of a high-intensity band at 370-440 nm arising from the presence of the coordinated esculetin photosensitizer ligand.

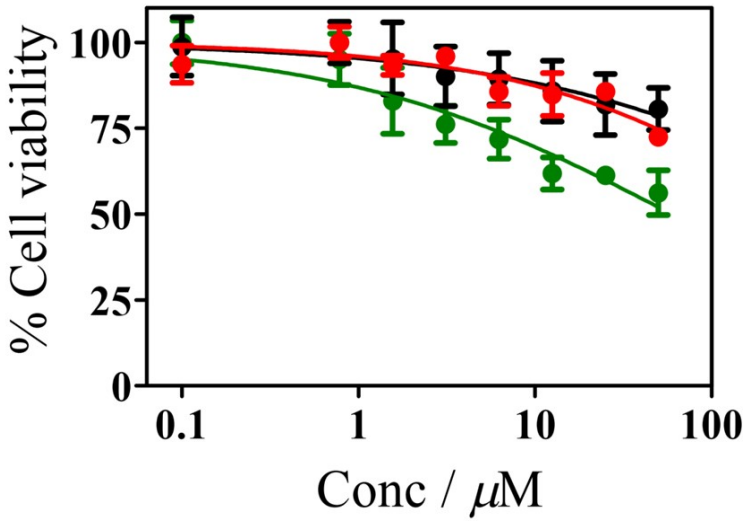

Fig. S16. Plots showing the cytotoxicity of complex **1a** against HeLa cervical cancer cells upon photo–irradiation with visible light (400–700 nm, 10 J cm^{-2}, green curve), red light (600-720 nm, 50 J cm^{-2}, red curve) and in the dark (black curve) as determined from the MTT assay.

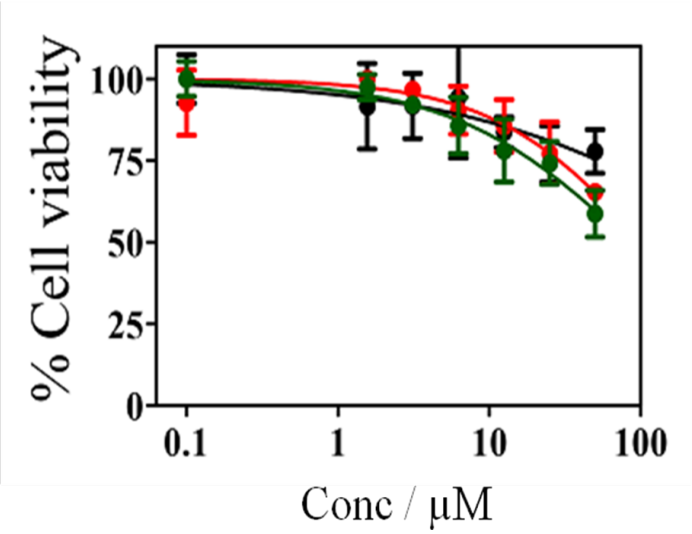

Fig. S17. Plots showing the cytotoxicity of complex **1a** against MCF-7 breast cancer cells upon photo–irradiation with visible light (400–700 nm, 10 J cm^{-2}, green curve), red light (600-720 nm, 50 J cm^{-2}, red curve) and in the dark (black curve) as determined from the MTT assay.

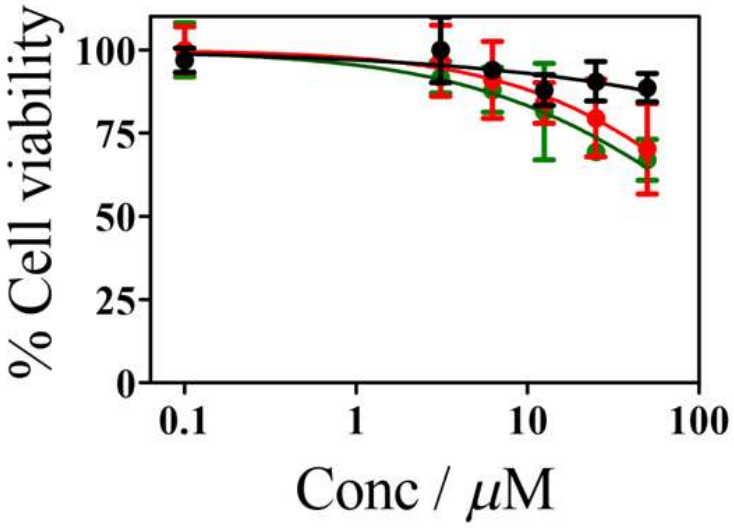

Fig. S18. Plots showing the cytotoxicity of complex **1a** against HaCaT, the human skin keratinocyte cells, upon photo–irradiation with visible light (400–700 nm, 10 J cm^{-2}, green curve), red light (600-720 nm, 50 J cm^{-2}, red curve) and in the dark (black curve) as determined from the MTT assay.

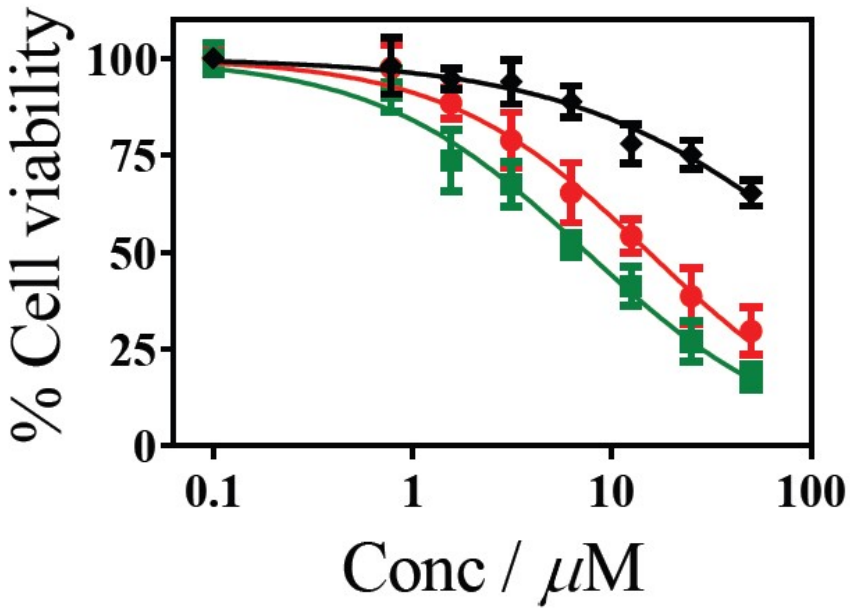

Fig. S19. Plots showing the cytotoxicity of complex **2a** against HeLa cervical cancer cells upon photo–irradiation with visible light (400–700 nm, 10 J cm^{-2}, green curve), red light (600-720 nm, 50 J cm^{-2}, red curve) and in the dark (black curve) as determined from the MTT assay.

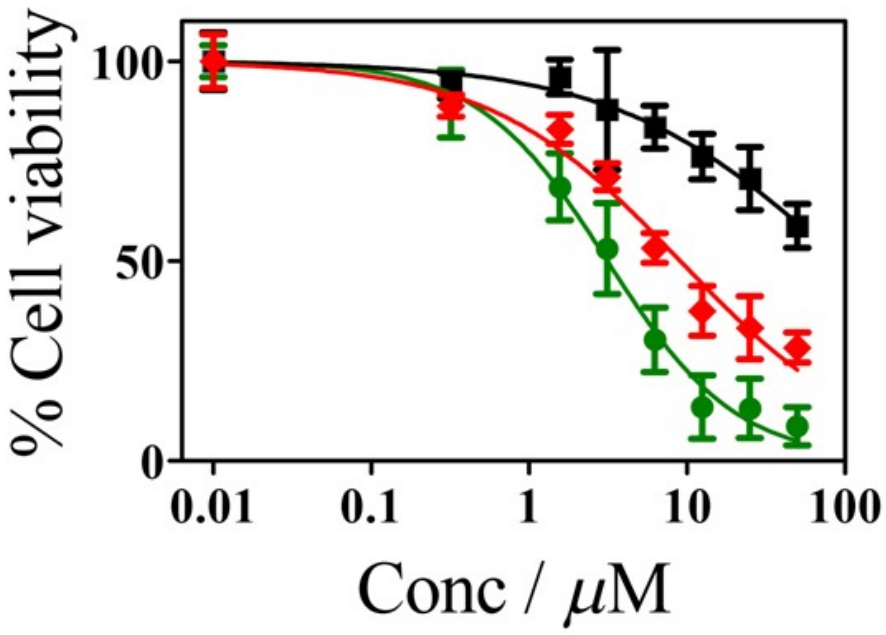

Fig. S20. Plots showing the cytotoxicity of complex **2a** against MCF-7 breast cancer cells upon photo–irradiation with visible light (400–700 nm, 10 J cm^{-2}, green curve), red light (600-720 nm, 50 J cm^{-2}, red curve) and in the dark (black curve) as determined from the MTT assay.

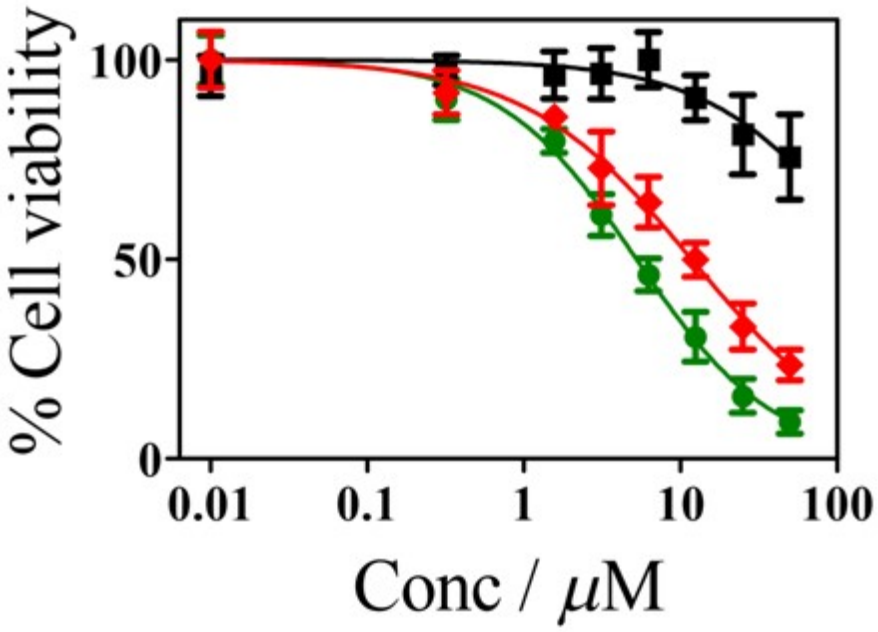

Fig. S21. Plots showing the cytotoxicity of complex **2a** against HaCaT, the human skin keratinocyte cells, upon photo–irradiation with visible light (400–700 nm, 10 J cm^{-2}, green curve), red light (600-720 nm, 50 J cm^{-2}, red curve) and in the dark (black curve) as determined from the MTT assay.

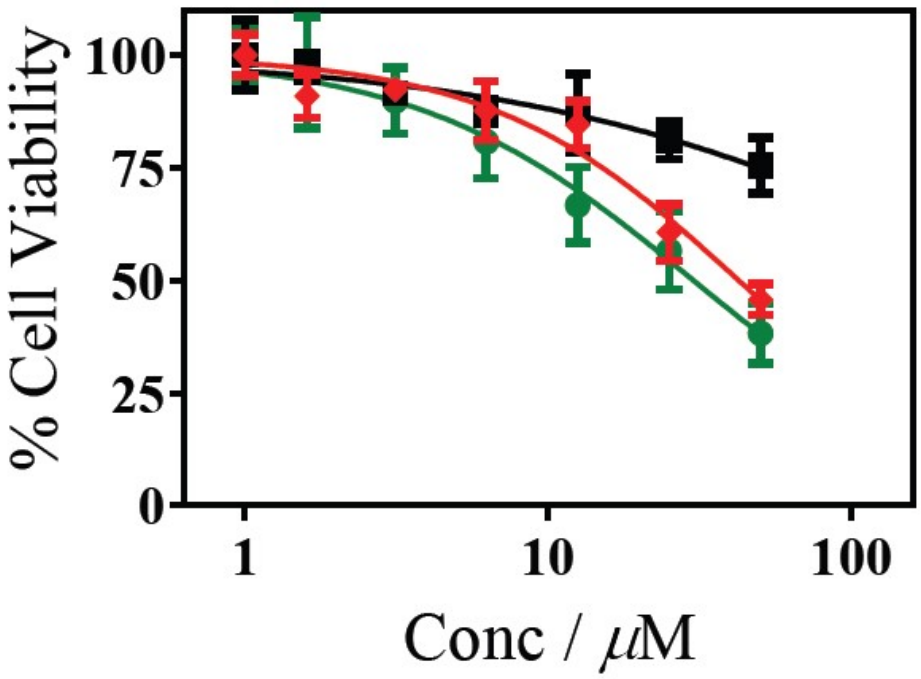

Fig. S22. Plots showing the cytotoxicity of complex **2a** against MCF-10A normal breast epithelial cells upon photo–irradiation with visible light (400–700 nm, 10 J cm^{-2}, green curve), red light (600-720 nm, 50 J cm^{-2}, red curve) and in the dark (black curve) as determined from the MTT assay.

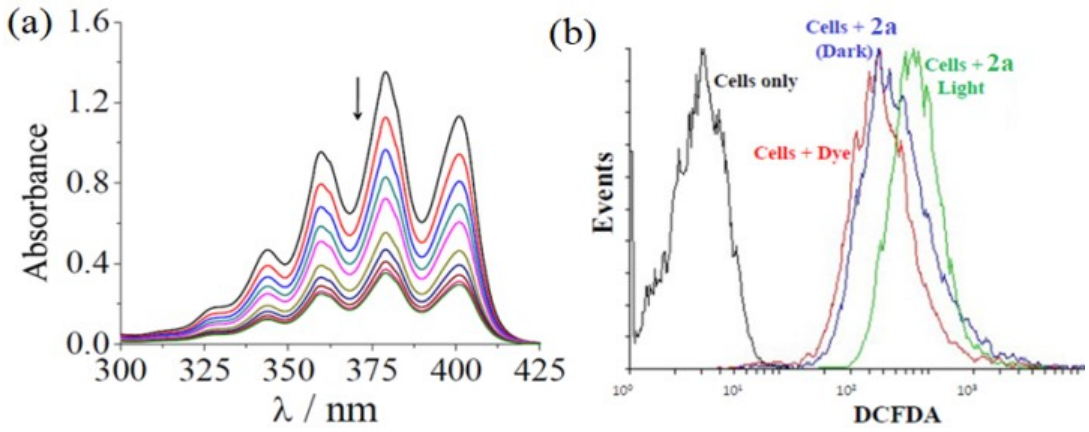

Fig. 23. (a) The absorption spectra of 9,10-anthracenediyl-bis(methylene)dimalonic acid (ABDA, 20 μM) in the presence of **2a** (10 μM of complex **2**) recorded at an interval of 10 min of continuous irradiation; (b) DCFDA assay showing the ROS generation by **2a** in HeLa cells. (Light source: visible light, 400–700 nm, 10 J cm^{-2}).

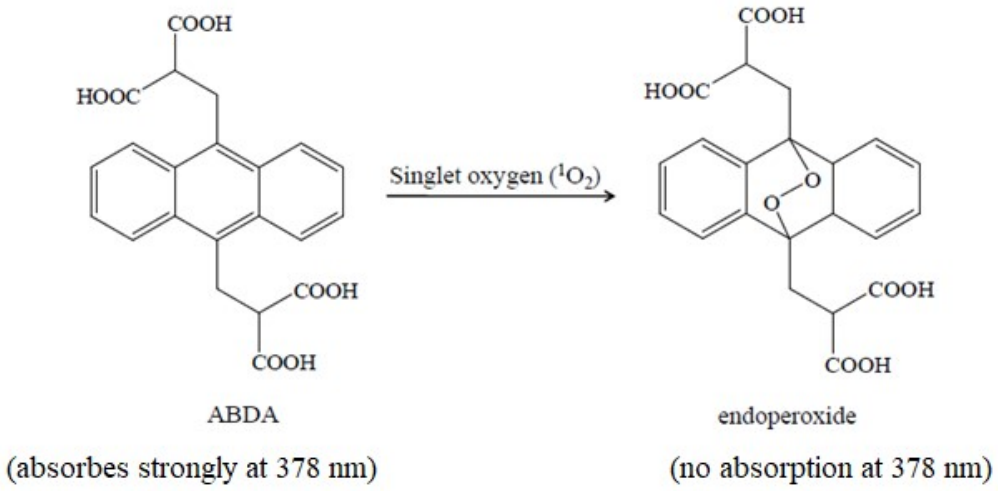

Fig. S24. Conversion of ABDA to endoperoxide by singlet oxygen. Note that ABDA absorbs strongly at 378 nm characteristic of anthracenyl chromophores. Upon conversion to endoperoxide, the absorption band disappears and consequently a decrease in absorbance of the band is observed.

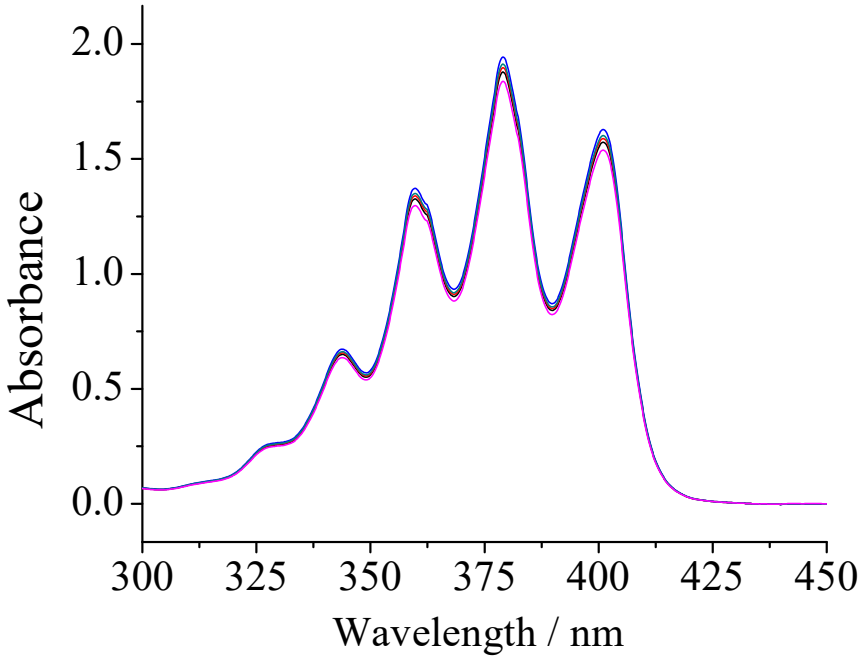

Fig. S25. The absorption spectra of 9,10-anthracenediyl-bis(methylene)dimalonic acid (ABDA, 20 μM) in 10% aqueous DMSO in the presence of complex **2a** (10 μM of complex **2**) and singlet oxygen quencher NaN_3 (0.5 mM) recorded at an interval of 10 min of continuous irradiation with visible light (400-700 nm, 10 J cm^{-2}) showing no noticeable changes.

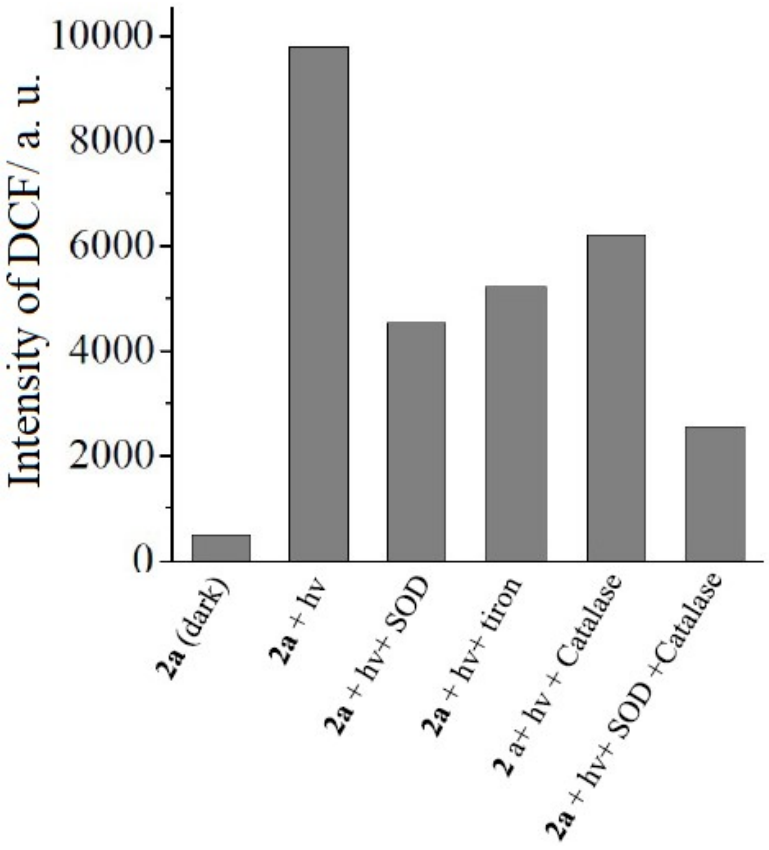

Fig. S26. Fluorescence intensity of DCF at 530 nm (excitation: 490 nm) under various experimental conditions suggesting the initial formation of the superoxide anion radical by red light irradiation of complex **2a (**20 μM of complex **2**) via a photoredox pathway and the subsequent formation of hydrogen peroxide by SOD (4 units) or tiron (0.5 mM).

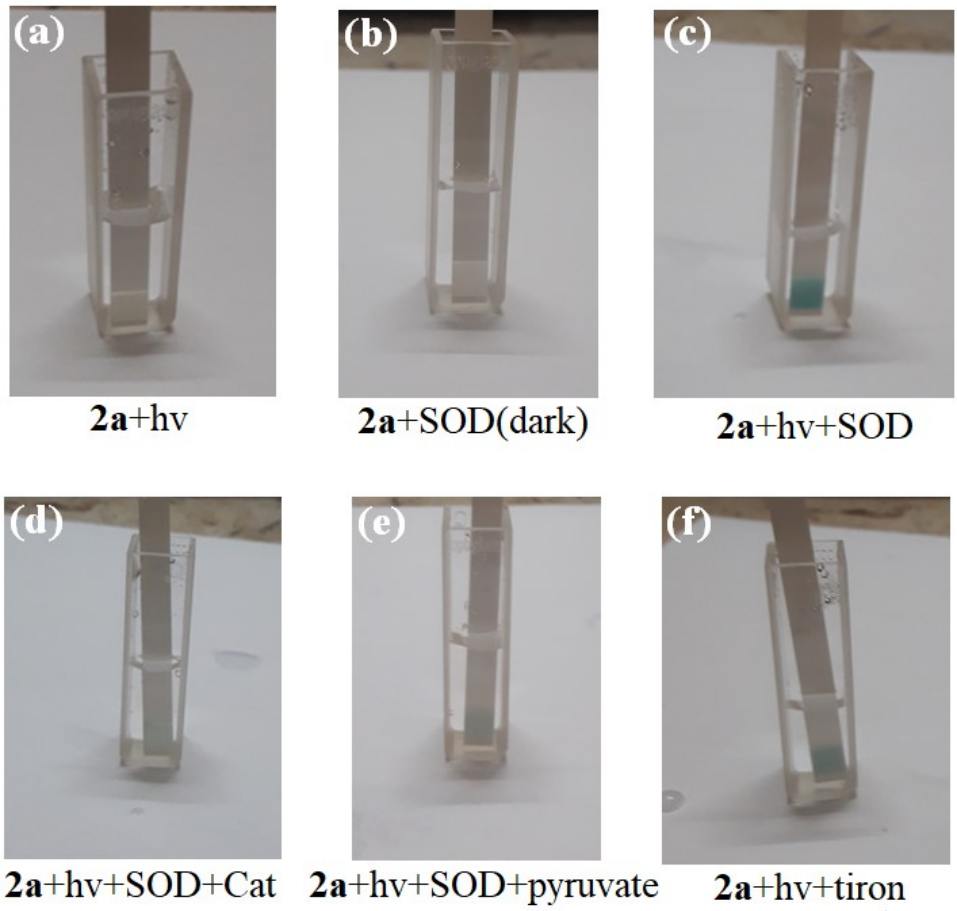

Fig. S27. Colorimetric peroxide stick test for the detection of hydrogen peroxide under various reaction conditions. (a) complex **2a** + red light, (b) complex **2a** + SOD (dark, 4 units), (c) complex **2a** + red light + SOD (4 units), (d) complex **2a** + red light + SOD +Catalase (4 units). (e) complex **2a** + red light + SOD + sodium pyruvate (0.5 mM), and (f) complex **2a** + red light + tiron (0.5 mM). Light Source: CW diode laser, wavelength: 705 nm, 38 mW). Concentration of complex **2** used: 10μM.

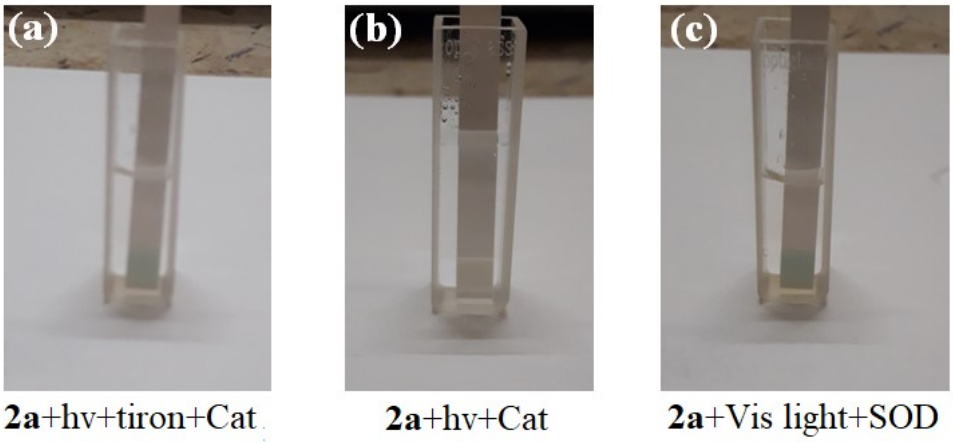

Fig. S28. Colorimetric peroxide stick test for the detection of hydrogen peroxide under various reaction conditions. (a) complex **2a** + red light +tiron (0.5 mM) + Catalase (4 units), (b) complex **2a** + red light + Catalase (4 units), and (c) complex **2a** + visible light + SOD (4 units). Red light source: CW diode laser, wavelength: 705 nm, 38 mW). Visible light source: Luzchem photoreactor, 400-700 nm, 10 J cm^{-2}). Concentration of complex **2** used: 10 μM.

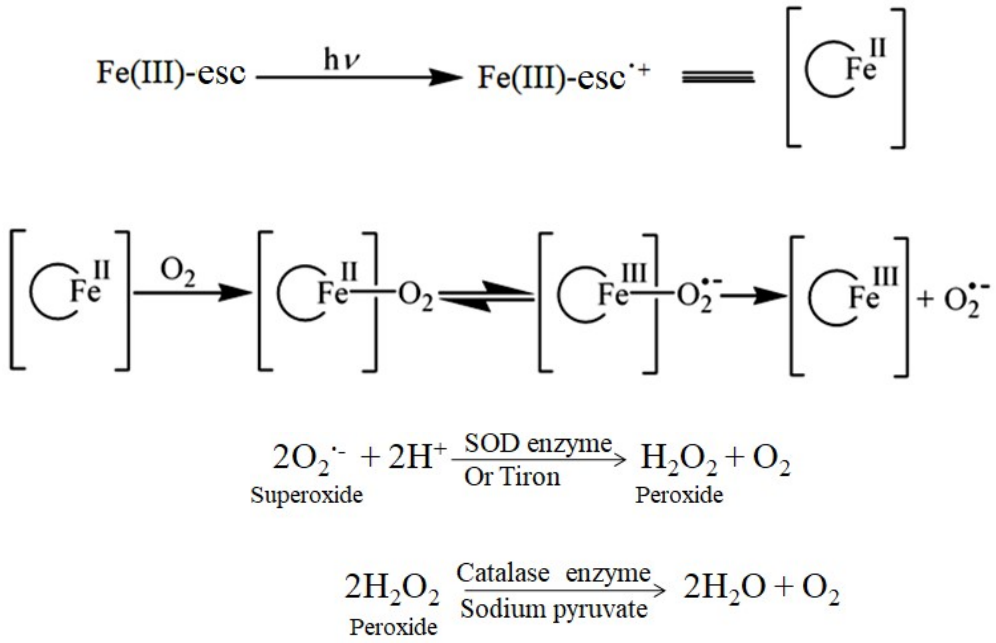

Fig. S29. Possible mechanism of initial formation of superoxide radical anion from complex **2a** on irradiation with red light (600-720 nm, 50 J cm^{-2}) in aqueous medium and the subsequent generation of hydrogen peroxide by SOD enzyme and final decomposition of hydrogen peroxide by catalase enzyme.

Table S1. Selected crystallographic data and structure refinement parameters for complex **1**.

Empirical formula	$C_{29}H_{27}N_3O_2ClFe_2$
Formula weight ($gmol^{-1}$)	596.68
Crystal system	Monoclinic
Space group	$P2_1/n$
a (Å)	11.2073(7)
b (Å)	19.5940(12)
c (Å)	11.9682(8)
α (°)	90
β (°)	98.963(4)
γ (°)	90
V ($Å^3$)	2596.1(3)
Z	4
T (K)	296(2)
ρ_{calc} (gcm^{-3})	1.515
λ/Å (Mo-K_α)	0.71073
μ (mm^{-1})	1.245
Data/restraints/parameters	7603/0/334
F(000)	1352
Goodness-of-fit on F^2	1.011
R (F_o)[a], I>2σ(I) / wR (F_o)[b]	0.0831/0.1223
R (all data)/wR (all data)	0.0430/0.1049
Largest diff. peak and hole (e $Å^{-3}$)	0.451, -0.649

[a] $R = \Sigma||F_o|-|F_c||/\Sigma|F_o|$. [b] $wR = \{\Sigma[w(F_o^2-F_c^2)^2]/\Sigma[w(F_o)^2]\}^{½}$; $w = [\sigma^2(F_o)^2 + (AP)^2 + BP]^{-1}$, where $P = (F_o^2 + 2F_c^2)/3$, A= 0.0570, B = 0.4624 for **1**.

Table S2. Selected bond distances (Å) and angles (°) in complex **1** with estimated standard deviations (e.s.d.) in the parentheses.

Fe(1)-N(1)	2.2992(19)	N(2)-Fe(1)-O(1)	85.45(7)
Fe(1)-N(2)	2.225(2)	N(2)-Fe(1)-O(2)	164.98(8)
Fe(1)-N(3)	2.166(2)	N(3)-Fe(1)-O(1)	159.68(8)
Fe(1)-O(1)	1.9423(19)	N(3)-Fe(1)-O(2)	86.14(7)
Fe(1)-O(2)	1.9603(16)	N(1)-Fe(1)-Cl(1)	154.91(5)
Fe(1)-Cl(1)	2.3251(9)	N(2)-Fe(1)-Cl(1)	90.55(6)
N(1)-Fe(1)-N(2)	73.07(7)	N(3)-Fe(1)-Cl(1)	91.01(6)
N(1)-Fe(1)-N(3)	74.48(7)	O(1)-Fe(1)-Cl(1)	108.01(6)
N(2)-Fe(1)-N(3)	101.83(8)	O(2)-Fe(1)-Cl(1)	102.13(6)
N(1)-Fe(1)-O(1)	89.90(8)	O(1)-Fe(1)-O(2)	83.00(7)
N(1)-Fe(1)-O(2)	97.28(7)		

Table S3: The optimized coordinates of the atoms in complex **1** obtained from DFT calculations**.**

Center Number	Atomic Number	Atomic Type	Coordinates (Angstroms) X	Y	Z
1	26	0	-1.979792	0.403973	0.098278
2	26	0	4.095164	-0.601187	-0.120242
3	17	0	-3.947167	1.722867	0.478580
4	7	0	-0.464564	-0.942288	-0.310832
5	8	0	-0.974706	1.543067	1.246209
6	8	0	-1.409857	1.552952	-1.312798
7	6	0	0.896562	-0.340248	0.032494
8	1	0	0.948020	0.603123	-0.514601
9	1	0	0.865592	-0.102457	1.097555
10	7	0	-2.289650	-0.782241	1.679536
11	7	0	-2.910257	-0.758164	-1.261687
12	6	0	-2.050613	-1.392765	-2.111833
13	6	0	-2.319435	-2.423977	3.948111
14	1	0	-2.327427	-3.059572	4.828213
15	6	0	-0.588511	-1.201799	-1.790893
16	1	0	0.003289	-2.070831	-2.096975
17	1	0	-0.211297	-0.315552	-2.308478

18	6	0	-1.518801	-1.905207	1.722363
19	6	0	-1.507112	-2.744867	2.847048
20	1	0	-0.875717	-3.627208	2.856108
21	6	0	2.076708	-1.219797	-0.290248
22	6	0	-0.559287	3.848449	-1.575239
23	1	0	-0.745919	3.842772	-2.647001
24	6	0	-3.068365	-0.460015	2.746721
25	1	0	-3.648122	0.449060	2.653093
26	6	0	-0.733073	-2.207543	0.471966
27	1	0	0.204184	-2.720650	0.704020
28	1	0	-1.320504	-2.889060	-0.153583
29	6	0	-0.648281	2.709317	0.605199
30	6	0	-0.887521	2.716298	-0.805885
31	6	0	2.784360	-2.070236	0.645140
32	1	0	2.541375	-2.191933	1.692333
33	6	0	2.747547	-1.336009	-1.569252
34	1	0	2.473506	-0.816469	-2.477236
35	6	0	-4.250823	-0.883996	-1.442391
36	1	0	-4.879901	-0.357411	-0.736648
37	6	0	0.242862	4.969980	0.454763
38	1	0	0.675823	5.844478	0.935411
39	6	0	-4.782951	-1.639067	-2.497794
40	1	0	-5.858639	-1.716285	-2.611395

41	6	0	-3.114201	-1.263167	3.894169
42	1	0	-3.751901	-0.976842	4.723275
43	6	0	-2.517490	-2.161344	-3.187226
44	1	0	-1.810330	-2.658315	-3.842927
45	6	0	-0.080181	3.835083	1.231938
46	1	0	0.099228	3.819476	2.304875
47	6	0	0.004887	4.976993	-0.938882
48	1	0	0.254813	5.856820	-1.527580
49	6	0	3.869950	-2.710821	-0.053501
50	1	0	4.580232	-3.403929	0.374896
51	6	0	5.951213	-0.075806	0.760617
52	1	0	6.664004	-0.778348	1.170111
53	6	0	3.845649	-2.257854	-1.423827
54	1	0	4.534203	-2.552493	-2.203321
55	6	0	4.156466	1.407334	0.559964
56	1	0	3.289507	2.010166	0.793072
57	6	0	-3.904232	-2.280885	-3.390165
58	1	0	-4.289217	-2.869442	-4.217191
59	6	0	4.796691	1.304760	-0.730233
60	1	0	4.496437	1.820830	-1.631682
61	6	0	4.870441	0.554722	1.481676
62	1	0	4.633812	0.409420	2.526700
63	6	0	5.905563	0.387385	-0.606718

64	1	0	6.576817	0.090664	-1.400755

Table S4: The optimized coordinates of the atoms in complex **2** obtained from DFT calculations.

Center Number	Atomic Number	Atomic Type	Coordinates (Angstroms) X	Y	Z
1	26	0	-1.853756	0.956658	0.171535
2	26	0	2.458384	-3.421261	-0.192403
3	17	0	-2.677362	3.128709	0.701567
4	7	0	-1.397921	-0.972303	-0.402435
5	8	0	-0.414653	1.170313	1.388882
6	8	0	-0.650801	1.695005	-1.142926
7	6	0	0.036593	-1.332700	-0.013991
8	1	0	0.666936	-0.552867	-0.445635
9	1	0	0.090033	-1.237546	1.072138
10	7	0	-2.850272	0.043189	1.632543
11	7	0	-3.223445	0.693880	-1.282819
12	6	0	-2.852900	-0.232455	-2.215591
13	6	0	-3.934682	-1.464157	3.725375
14	1	0	-4.352576	-2.050183	4.538040

15	6	0	-1.574379	-0.968875	-1.900464
16	1	0	-1.589998	-1.987569	-2.301216
17	1	0	-0.723188	-0.433215	-2.329585
18	6	0	-2.903839	-1.315425	1.540093
19	6	0	-3.437131	-2.099245	2.574409
20	1	0	-3.459018	-3.179562	2.476854
21	6	0	0.490770	-2.695700	-0.466939
22	6	0	1.369841	3.060570	-1.208133
23	1	0	1.273453	3.276140	-2.267149
24	6	0	-3.316669	0.663324	2.749015
25	1	0	-3.231462	1.741906	2.764568
26	6	0	-2.402661	-1.899741	0.244911
27	1	0	-1.966637	-2.890772	0.394657
28	1	0	-3.251747	-2.026147	-0.435639
29	6	0	0.555415	1.985684	0.869986
30	6	0	0.418243	2.267941	-0.541329
31	6	0	0.470659	-3.912048	0.320525
32	1	0	0.104252	-4.001712	1.334425
33	6	0	1.087551	-3.020664	-1.746574
34	1	0	1.260388	-2.326987	-2.558099
35	6	0	-4.375703	1.394290	-1.447963
36	1	0	-4.615125	2.113120	-0.675575
37	6	0	2.604562	3.305970	0.926380

38	6	0	-5.194721	1.204938	-2.570381
39	1	0	-6.107607	1.781664	-2.669329
40	6	0	-3.873369	-0.060244	3.811737
41	1	0	-4.240067	0.468024	4.684819
42	6	0	-3.624941	-0.466134	-3.361459
43	1	0	-3.307977	-1.211155	-4.083584
44	6	0	1.633431	2.498431	1.587547
45	1	0	1.735306	2.284709	2.648464
46	6	0	2.443999	3.564817	-0.464373
47	6	0	1.038089	-4.974224	-0.470795
48	1	0	1.163498	-6.001373	-0.158398
49	6	0	4.178393	-4.225655	0.750229
50	1	0	4.306059	-5.263943	1.023883
51	6	0	1.418074	-4.422829	-1.749548
52	1	0	1.878697	-4.964149	-2.563944
53	6	0	3.609842	-1.960440	0.827412
54	1	0	3.238440	-1.004379	1.170218
55	6	0	-4.810045	0.268413	-3.547807
56	1	0	-5.423938	0.105095	-4.428113
57	6	0	4.192598	-2.230309	-0.466147
58	1	0	4.333940	-1.511851	-1.261784
59	6	0	3.601612	-3.193434	1.579405
60	1	0	3.223147	-3.322850	2.583958

61	6	0	4.543268	-3.630516	-0.514151
62	1	0	4.991231	-4.145251	-1.353009
63	6	0	3.746631	3.878220	1.584335
64	6	0	4.662491	4.652074	0.906223
65	6	0	4.517741	4.928624	-0.507515
66	1	0	3.885597	3.690324	2.646260
67	1	0	5.525667	5.084608	1.398364
68	8	0	3.383382	4.357467	-1.146222
69	8	0	5.279125	5.613862	-1.230635

Table S5. IC_{50} (μM) values for complexes **1a** and **2a**, esculetin ligand and the clinical drug Photofrin against various cell lines as determined from the MTT assay.[a]

Cell lines	**1a**		**2a**		Esculetin		Photofrin[b]	
	Dark	Light	Dark	Light	Dark	Light	Dark	Light
MCF-7	>50	>50 (>50)	>50	8.8±1.3 (3.2±0.8)	13.6±1.2	(11.4±1.3)	-	-
HeLa	>50	>50 (>50)	>50	15.3±1.1(7.4±1.0)	20.3±1.4	(18.2±1.5)	>41	4.3±0.2
HaCaT	>50	>50 (>50)	>50	11.8±1.7(5.1±1.1)	17.8±1.1	(15.4±1.6)	-	-
MCF-10A	-	-	>50	>42 (31.6±2.7)	28.4±2.1	(25.3±1.9)	-	-

[a]Cells incubated with compound for 4 h in the dark followed by irradiation with red light (600-720 nm, Waldman PDT 1200L, 50 J cm^{-2}). IC_{50} values in the parenthesis correspond to visible light (400-700 nm, 10 J cm^{-2}, Luzchem photoreactor). The complex [Fe(L)(cat)(NO_3)] is reported to give IC_{50} values of 18.8±0.1μM in red light and 6.2±0.1μM in visible light against HeLa cells and 11.3±0.1μM in visible light against MCF-7 cells under similar experimental conditions (IC_{50} in dark is >100 μM) (reference 7a in the manuscript). [b]Reference 21in the manuscript. For the IC_{50} values, the concentrations of complexes **1** and **2** are to be considered.

References

(S1) D. D. Perrin, W. L. F. Armarego and D. R. Perrin, *Purification of Laboratory Chemicals*; Pergamon Press: Oxford, 1980.

(S2) A. J. Evans, S. E. Watkins, D. C. Craig and S. B. Colbran, *J. Chem. Soc. Dalton Trans*., 2002, 983.

(S3) J. Guilford II, R. Jackson, C. Choi and W. R. Bergmark, *J. Phys. Chem.,* 1985, **89**, 294.

(S4) J. R. Lakowicz in *Principles of Fluorescence Spectroscopy*, Kluwer Academic/Plenum Publishers, New York, 1999.

(S5) A. T. R. Williams, S. A. Winfield and J. N. Miller, *Analyst,* 1983, **108**, 1067.

(S6) D. F. Evans, *J. Chem. Soc*., 1961, 1987.

(S7) T. Sarkar, S. Banerjee and A. Hussain, *RSC Advances,* 2015, **5**, 29276.

(S8) D. F. Evans, *J. Chem. Soc.,* 1959, 2003.

(S9) J. Wu, D. G. J. Goodwin, K. Peter, D. Benoit, W. Li, D. H. Fairbrother and J. D. Fortner, *Environ. Sci. Technol. Lett.,* 2014, **1**, 490.

(S10) N. Walker and D. Stuart, *Acta Crystallogr.,* 1983, **A39**, 158.

(S11) (a) G.M. Sheldrick, *Acta Crystallogr. Sect. A,* 2008, **64***,* 112; (b) L. J. Farrugia, *J. Appl. Crystallogr.,* 1999, **32**, 837.

(S12) C. K. Johnson, *ORTEP, Report ORNL-5138*; Oak Ridge National Laboratory: Oak Ridge, TN, 1976.

(S13) (a) A. D. Becke, *Phys. Rev*., 1998, **A38**, 3098. (b) A. D. Becke, *J. Chem. Phys*., 1993, **98**, 5648. (c) C. Lee, W. Yang and R. G. Parr, *Phys. Rev. B*., 1988, **37**, 785.

(S14) M. J. Frisch, G. W. Trucks, H. B. Schlegel, G. E. Scuseria, M. A. Robb, J. R. Cheeseman, J.A. Montgomery, T. Vreven, K. N. Kudin, J. C. Burant, J. M. Millam, S. S. Iyengar, J. Tomasi, V. Barone, B. Mennucci, M. Cossi, G. Scalmani, N. Rega, G. A. Petersson, H. Nakatsuji, M. Hada, M. Ehara, K. Toyota, R. Fukuda, J. Hasegawa, H. Ishida,

T. Nakajima, Y. Honda, O. Kitao, H. Nakai, M. Klene, X. Li, J. E. Knox, H. P. Hratchian, J. B. Cross, C. Adamo, J. Jaramillo, R.Gomperts, R. E. Stratmann, O. Yazyev, A. J. Austin, R. Cammi, C. Pomelli, J. Ochterski, P. Y. Ayala, K. Morokuma, G. A. Voth, P. Salvador, J. J. Dannenberg, V. G. Zakrzewski, S. Dapprich, A. D. Daniels, M. C. Strain, O. Farkas, D. K. Malick, A. D. Rabuck, K. Raghavachari, J. B. Foresman, J. V. Ortiz, Q. Cui, A. G. Baboul, S. Clifford, J. Cioslowski, B. B. Stefanov, G. Liu, A. Liashenko, P. Piskorz, I. Komaromi, R. L. Martin, D. J. Fox, T. Keith, M. A. Al-Laham, C. Y. Peng, A. Nanayakkara, M. Challacombe, P. M. W. Gill, B. Johnson, W. Chen, M. W. Wong, C. Gonzalez and J. A. Pople, Gaussian 03, revision B.4; Gaussian Inc.: Pittsburgh, PA, 2003.

(S15) T. Mosmann, *J. Immunol. Methods,* 1983, **65**, 55.

(S16) Y. Yuan, C.-J. Zhang, S. Xu and B. Liu, *Chem. Commun.,* 2015, **51**, 8626.

(S17] A. S. Keston and R. Brandt, *Anal. Biochem*., 1965, **11**, 1.

(S18) T. Takanashi, Y. Ogura, H. Taguchi, M. Hashizoe and Y. Honda, *Invest. Ophthalmol. Vis. Sci*., 1997, **38**, 2721.

(S19) S. Banerjee, K. A. Dixit, S. Maheswaramma, B. Maity, S. Mukherjee, A. Kumar, A. Karande and A. R. Chakravarty, *J. Chem. Sci*., 2016, **128**, 165.

(S20) T. Mukherjee, A. Dixit, S. Banerjee, A. A. Karande and A. R. Chakravarty, *J. Ind. Chem. Soc*., 2015, **92**, 1855.

(S21) K. Apel and H. Hirt, *Annu. Rev. Plant Biol.,* 2004, **55**, 373.

(S22) V. Novohradsky, G. Vigueras, J. Pracharova,N. Cutillas, C. Janiak, H. Kostrhunova, V. Brabec, J. Ruiz and J. Kasparkova, *Inorg. Chem. Front.,* 2019, **6**, 2500.

(S23) N. M. Martin, A. Friedlander, A. Mok, D. Kent, M. Wiedmann and K. J. Boor, *J. Food Prot.,* 2014, **77**, 1809.

(S24) N. Anitha and M. Palaniandavar, *Dalton Trans.*, 2011, **40**, 1888.

(S25) K. Sundaravel, E. Suresh, K. Saminathan and M. Palaniandavar, *Dalton Trans.,* 2011, **40**, 8092.

(S26) P. Prasad, I. Khan, P. Kondaiah and A. R. Chakravarty, *Chem. Eur. J.,* 2013, **19**, 17445.

(S27) P. Prasad, P. K. Sasmal, I. Khan, P. Kondaiah and A. R. Chakravarty, *Inorg. Chim. Acta*, 2011, **372**, 79.

(S28) S. Banerjee, A. Hussain, P. Prasad, I. Khan, B. Banik, P. Kondaiah and A. R. Chakravarty, *Eur. J. Inorg. Chem.,* 2012, 3899.

(S29) U. Basu, I. Khan, A. Hussain, B. Gole, P. Kondaiah and A. R. Chakravarty, *Inorg. Chem.,* 2014, **53**, 2152.

(S30) D. D. Cox, S. J. Benkovic, L. M. Bloom, F. C. Bradley, M. J. Nelson, L. Que, Jr. and D. E. Wallickt, *J. Am. Chem. Soc.,* 1988, **110**, 7, 2026.